

NASA CR-1942

NASA CONTRACTOR
REPORT



NASA CR-1

C. I.

00000000000000000000000000000000
TECH LIBRARY KAFB, NM
Barcode

LOAN COPY: RETURN TO
AFWL (DO L)
KIRTLAND AFB, N. M.

DETERMINATION OF STRATOSPHERIC
TEMPERATURE AND HEIGHT GRADIENTS
FROM NIMBUS III RADIATION DATA

by G. W. Nicholas, D. N. Hovland, and A. D. Belmont

Prepared by

CONTROL DATA CORPORATION

Minneapolis, Minn. 55440

for George C. Marshall Space Flight Center

NATIONAL AERONAUTICS AND SPACE ADMINISTRATION • WASHINGTON, D. C. • NOVEMBER 1971



0060993

1. REPORT NO. NASA CR-1942	2. GOVERNMENT ACCESSION NO.	3. RECEIVED	
4. TITLE AND SUBTITLE DETERMINATION OF STRATOSPHERIC TEMPERATURE AND HEIGHT GRADIENTS FROM NIMBUS III RADIATION DATA		5. REPORT DATE November 1971	
7. AUTHOR(S) G. W. Nicholas, D. N. Hovland, and A. D. Belmont		6. PERFORMING ORGANIZATION CODE	
9. PERFORMING ORGANIZATION NAME AND ADDRESS Control Data Corporation 8100 South 34th Avenue Minneapolis, Minnesota 55440		8. PERFORMING ORGANIZATION REPORT #	
12. SPONSORING AGENCY NAME AND ADDRESS NASA Washington, D. C. 20546		10. WORK UNIT NO.	
		11. CONTRACT OR GRANT NO. NAS8-25949	
		13. TYPE OF REPORT & PERIOD COVERED CONTRACTOR REPORT	
15. SUPPLEMENTARY NOTES			
16. ABSTRACT <p>To improve the specification of stratospheric horizontal temperature and geopotential height fields from satellite radiation data, needed for high flying aircraft, a technique has been derived to estimate data between satellite tracks using interpolated IRIS 15-micron data from Nimbus III. The interpolation is based on the observed gradients of the MRIR 15-micron radiances between subsatellite tracks. The technique was verified with radiosonde data taken within 6 hours of the satellite data. The sample varied from 1126 pairs at low levels to 383 pairs at 10 mb using northern hemisphere data for June 15 to July 20, 1969. The data were separated into five latitude bands. The RMS temperature differences were generally from 2 to 5 C for all levels above 300 mb. From 500 to 300 mb RMS differences vary from 4 to 9C except at high latitudes which showed values near 3C. The RMS differences between radiosonde heights and those calculated hydrostatically from the surface were from 30 to 280 meters increasing from the surface to 10 mb. Integration starting at 100 mb reduced the RMS difference in the stratosphere to 20 to 120 meters from 70 to 10 mb. From a comparison with actual operational maps at 50 and 10 mb, it appears the techniques developed here produce analyses in general agreement with those from radiosonde data. In addition, they are able to indicate details over areas of sparse data not shown by conventional techniques.</p>			
17. KEY WORDS Stratospheric horizontal temperature fields, stratospheric horizontal geopotential height fields, IRIS data, MRIR data.		18. DISTRIBUTION STATEMENT	
19. SECURITY CLASSIF. (of this report) UNCLASSIFIED	20. SECURITY CLASSIF. (of this page) UNCLASSIFIED	21. NO. OF PAGES 65	22. PRICE \$3.00

This report was prepared by Control Data Corporation under Contract NAS8-25949 "Application of 15-micron Data from Nimbus III to Stratospheric Circulation" for the George C. Marshall Space Flight Center of the National Aeronautics and Space Administration. The work was administered under the technical direction of the Aero-Astrodynamic Laboratory of the George C. Marshall Space Flight Center.

TABLE OF CONTENTS

1.0	<u>INTRODUCTION</u>	1
2.0	<u>THEORY</u>	3
2.1	Radiative Transfer in the Atmosphere	3
2.2	Weighting Curves	4
2.3	Methods to Derive Temperature Profiles	6
2.4	Geopotential Heights	7
3.0	<u>DATA</u>	8
4.0	<u>INTERPOLATION PROCEDURE</u>	12
5.0	<u>RESULTS</u>	19
5.1	Plotted Comparison of Radiosonde to IRIS Temperature Profiles	19
5.2	Verification Statistics	21
5.3	Comparison with NMC Maps	26
5.4	Sources of Errors	30
6.0	<u>SUMMARY AND CONCLUSIONS</u>	32
7.0	<u>REFERENCES</u>	35
	APPENDIX A <u>DATA PROCESSING</u>	37
A.1.0	Radiosondes	37
A.2.0	IRIS Data	39
A.3.0	MRIR Data	39
A.4.0	Processing to Locate Corresponding Sets	40
	APPENDIX B <u>CORRECTIONS FOR CLOUDS AND HOT TERRAIN</u>	42

Figures 1 through 16 and Tables 1 and 2 follow Appendix B

LIST OF FIGURES

<u>Figure</u>	<u>Title</u>
1.	Atmospheric weighting functions
2.	An example of the interpolation scheme
3.	Comparison of IRIS derived temperature profile and Guantanomo, Cuba radiosonde
4.	Comparison of IRIS derived temperature profile and Shionomisaki, Japan radiosonde
5.	Comparison of IRIS derived temperature profile and Maniwaki, Quebec radiosonde
6.	Comparison of IRIS derived temperature profile and Sodankyla, Finland radiosonde
7.	RMS temperature differences
8.	Absolute temperature differences
9.	RMS height differences
10.	Absolute height differences
11.	NMC 100 mb map
12.	IRIS derived 100-mb map
13.	NMC 50-mb map
14.	IRIS derived 50-mb map
15.	NMC 10-mb map
16.	IRIS derived 10-mb map

LIST OF TABLES

<u>Table</u>	<u>Title</u>
1.	Correlations of IRIS derived and radiosonde temperatures.
2.	Correlations of IRIS derived and radiosonde heights.

1.0 INTRODUCTION

The efficiency of high flying aircraft is strongly dependent upon the temperature and wind field and especially the horizontal gradients of these fields along the flight route. The best source of upper-air data now is satellite radiation observations which make it possible to derive the vertical profiles of temperature on a global basis. However, such data are limited to points along the subsatellite tracks which are 3000 km apart at the equator, or to two additional points between tracks (for SIRS B). The purpose of this study is, therefore, to find a method of estimating the values at any location between tracks thus increasing the horizontal resolution of the radiation data for the particular case of Nimbus III IRIS observations. The result is a more detailed estimate of the horizontal gradient, at each pressure level, of the temperature and height fields from which winds can be derived.

Nimbus III carried two experiments in which the spectral radiances in relatively narrow intervals were obtained and from which temperature profiles can be derived. One of these was the Infrared Interferometer Spectrometer, IRIS, which is described by Conrath, et al (1970), and Hanel, et al (1970). Briefly, the IRIS measures the radiances in narrow (5 cm^{-1}) spectral intervals from 400 to 2000 cm^{-1} (5 to 25-micron). For the research reported here use was made of only two portions, the CO_2 band at 667 cm^{-1} and the atmospheric window at 900 cm^{-1} . In addition to the spectrometers,

Nimbus III also carried a Medium Resolution Infrared Radiometer, MRIR.

This instrument is a five-channel scanning radiometer. It, or variations of it, has been used on meteorological satellites since TIROS II and has been described in the Nimbus III User's Guide. The five wave length regions are fairly broad. The one which concerns us here is the 645- 690 cm^{-1} (15-micron) CO_2 absorption band.

The IRIS on Nimbus III viewed only in the nadir direction, resulting in coverage only along the subsatellite track. The MRIR mirror, on the other hand, scanned from horizon to horizon resulting in complete coverage between subsatellite tracks. The MRIR 15-micron channel overlapped some of the IRIS frequencies used to derive temperature profiles. The gradients of the MRIR 15-micron radiance between tracks should thus reflect, to a reasonable degree, the horizontal temperature gradients sampled at subsatellite intervals by the IRIS 15-micron spectral data, at levels for which there is considerable overlap in the weighting curves (Figure 1). For the less opaque spectral intervals that are weighted heavily in the lower troposphere and whose weighting curves overlap very little with the MRIR weighting curve, the IRIS gradients correlate less with MRIR gradients. There is not complete correspondence between these gradients, of course, as many different temperature distributions can result in the same value of the MRIR 15-micron radiance. However, the research reported here was based on the premise that the atmosphere changes in a reasonably ordered manner, at least over the distances between orbits, over the time between orbits and in the part of the atmosphere of interest, i.e., the stratosphere.

2.0 THEORY

2.1 Radiative Transfer in the Atmosphere

The radiances received at the satellite depend on the emission, absorption, and scattering of the intervening atmosphere, as well as on the emission and reflection of earth's surface. If scattering in the atmosphere and reflection of the surface are neglected, the spectral radiance can be expressed as

$$I(\nu) = \epsilon_s B[\nu, T_s(P_s)] \tau_s(\nu, P_s) - \int_{P_t}^{P_s} B[\nu, T(p)] \frac{\partial \tau(\nu, p)}{\partial \ln p} d\ln p \quad (1)$$

The first term on the right of (1) is the component of radiation emitted by the surface (cloud or ground) at temperature T_s .

τ_s is the atmospheric transmission at the surface and ϵ_s is the emissivity of surface and is assumed to be unity for this work.

$B(\nu, T_s)$ is the Planck radiance. The second term is the contribution to the radiance by direct emission of the atmosphere. The logarithm of pressure has been chosen as the independent height related variable. The pressure level P_t is the top of the atmosphere above which the atmospheric contribution to the radiance is negligible. P_t is taken as 0.1 mb in this report. $B[\nu, T(p)]$ is the Planck radiance and $\partial \tau(\nu, p)/\partial (\ln p)$ is the change of transmission with change of pressure, called the weighting function.

The second term on the right of Eq. (1) is by far the most important term for vertical sounding although the first term is not

negligible for some spectral intervals. The first term dominates in determining the surface temperature.

2.2 Weighting Curves

The spectral transmittance τ of an atmospheric gas between the pressure level, p , and the satellite is

$$\tau_i(\nu, p) = \exp \left[-\frac{1}{g} \int_0^p k_i(\nu, p) q_i(p) dp \right] \quad (2)$$

where g is the acceleration of gravity, and k_i is the absorption coefficient of constituent i . The mixing ratio of that constituent is q_i . For the work reported here, the transmittances used were those reported by Smith (1969) in which he used a polynomial to fit the experimentally determined transmission values for the 15-micron CO_2 and the rotational H_2O data. Smith's tabulated regression coefficients are for 5 cm^{-1} spectral intervals.

It was found that these CO_2 transmittances were somewhat too large. Often the absorption coefficients are determined by laboratory work using generally much shorter path lengths than found in the atmosphere. As a consequence, when the laboratory measurements are extrapolated to atmospheric conditions errors occur. The transmittances were adjusted by shifting τ along the pressure ordinate until the computed radiance using radiosonde soundings equaled the corresponding measured radiances for the spectral intervals of IRIS. Over 100 pairs of cloud-free radiosondes and IRIS radiance sets were used to derive this pressure adjustment factor; all computed transmittances were based on the value of this factor.

If temperature is known then $\frac{\partial \tau}{\partial \ln p}$ can be computed and the weighting curves constructed. The weighting curves corresponding to the 5 cm^{-1} spectral intervals used in this study are shown in Figure 1. In the selection of the eleven 5 cm^{-1} spectral intervals, all of the weighting curves from 667.5 to 757.5 cm^{-1} were calculated and plotted. It was found that for wave numbers of 717.5 cm^{-1} and longer, the weighting curve shifted to higher layers in the atmosphere and then shifted to lower layers duplicating the smaller wave number weighting curves. For the spectral resolution in the 5 cm^{-1} spectral interval representation of the transmittances used here very little vertical resolution can be obtained in the weighting curves for intervals between 712.5 to 757.5 cm^{-1} . B. Conrath * (private communication, 1971) has been able to show that better vertical resolution of the weighting curves is possible in this region of the atmosphere by using another method of resolving the spectral lines for the calculation of τ .

Figure 1 shows that various layers of the atmosphere are weighted differently in different spectral intervals. In principle, the temperature can be determined from Eq. (1) if the radiance is known. Thus, by measuring in several spectral intervals from the strongly absorbing center (667.5 cm^{-1}) of the CO_2 band, to the weakly absorbing wing (757.5 cm^{-1}), several temperatures can be determined representing different layers in the vertical such as those shown in Figure 1. However, in practice, this approach results in unstable solutions because of the overlap in the weighting curves and the sensitivity to random errors in the measurements.

*Dr. Barney Conrath, Radiations Branch, NASA-Goddard Space Flight Center, Greenbelt, Maryland.

2.3 Methods to derive temperature profiles.

Since it was first suggested by King (1958) and Kaplan (1959) that temperature profiles could be obtained from spectral measurements in the CO₂ bands much work has been done to develop techniques resulting in stable, physically meaningful temperature profiles (King (1964), Wark and Fleming (1966), Rodgers (1966), Strand and Westwater (1968), Chahine (1968 and 1970), Barnett (1969), and Smith (1970)). These methods can be divided into two general classes: One is a statistical technique which relies on the correlation of the behavior of the temperature profile, usually radiosondes, and the behavior of corresponding measured radiances. The other one is an iterative estimation technique which employs only the measured radiances; however, it does require knowledge of the water vapor distribution and a surface temperature.

The latter technique was employed in this research, one proposed by Chahine (1968) and applied successfully by Conrath, et al (1970). In this method the temperature profile is represented by the temperature T_i (i=1,...,M) for M predetermined anchor pressure levels. Each anchor level is paired to a given spectral interval, and the radiance associated with that level is calculated from

$$B(\nu_i, T_i^{n+1}) = \left[\frac{\tilde{I}(\nu_i) - B(\nu_i, T_s) \tau(\nu_i, P_s)}{I^n(\nu_i) - B(\nu_i, T_s) \tau(\nu_i, P_s)} \right] B(\nu_i, T_i^n) \quad (3)$$

where T_iⁿ⁺¹ is the (n+1)st estimate of T_i and Iⁿ(ν_i) is the computed radiance from Eq.(1) using the nth estimate of the temperature profile

consisting of linearly interpolated temperatures between anchor levels. The measured radiances from IRIS are designated by $\tilde{I}(\nu_i)$. A first guess of a temperature profile is required to start the iterative scheme. The iteration is continued until the RMS difference between the calculated and measured radiances is less than a preset value.

The selection of the anchor pressure levels was made by requiring them to be at or near the level of the peaks of the weighting curves. Five July standard atmospheres (U.S. Standard Atmosphere, Supplement, 1966) representing five latitude bands were used to calculate the weighting functions. The latitude bands are $0-22.5^\circ$, $22.5-37.5^\circ$, $37.5-52.5^\circ$, $52.5-67.5^\circ$, and $67.5^\circ-90^\circ$. Small deviations from the weighting curve peaks were allowed to improve the definition of certain expected characteristics of the temperature profile; mainly, the improved definition of the tropopause. When the data were being processed, a different set of anchor levels was used for each latitude band.

2.4 Geopotential Height.

Once the pressure-temperature relations are derived by the iterative technique, the geopotential height can be determined from the hydrostatic equation. The height at some pressure level must be known to start the integration. For our work the initial heights were specified from nearby radiosondes. From the gradient of the horizontal height field determined from many temperature profiles, the geostrophic wind field can be specified.

3.0 DATA

Three types of data were used in this study: MRIR 15-micron and IRIS radiation data both from Nimbus III, and radiosonde data. The 35-day period for which data were analyzed was June 15 to July 20, 1969. This period was dictated because it was the only time for which IRIS data were available when this study began. These data had been reduced and formatted on tape for another requirement, and they were made available for this study.

Because the winter stratosphere has much larger horizontal temperature and geopotential height gradients than the summer stratosphere, it would have been more desirable to use winter data. The IRIS of Nimbus III lasted only from launch on April 14 to July 20, 1969, and therefore winter data for the nothern hemisphere were never recorded.

Unfortunately, the IRIS data that were available were noisy. The random noise was caused by electrical interference initiated during the playback mode. The noise was lessened in magnitude and frequency with time after each playback, so that until just prior to playback again, the data were relatively free of noise. No attempt was made to use only the relatively good data; however, all data were smoothed spectrally and averaged spatially during the interpolation process.

The IRIS instrument had a field-of-view of 150 km on a side, and it viewed only in the zero nadir direction. The MRIR, on the other hand, had a field-of-view of 60 km diameter and scanned from

horizon to horizon perpendicular to the subsatellite track. The sampling rate and the forward motion of the satellite provided contiguous viewed spots in all directions. Very nearly 2.5 MRIR viewed spots fall along the IRIS viewed spot dimension. This distance is nearly 2 times 0.65° latitude or 2 times 0.65° longitude divided by the cosine of the latitude. Thus, the MRIR 15-micron values located within this distance of the IRIS center location were averaged and used with the IRIS values. The same procedure was also used to find an average MRIR 15-micron value for the radiosonde location.

The radiosondes serve four purposes in this work. First, they provide water vapor and surface temperature information necessary to the solution of the radiative transfer equation during the iterative procedures of deriving temperature profiles. The surface (shelter) temperature is necessary to determine if clouds are in the field-of-view. Second, the radiosonde temperature profile and its vertical extrapolation above recorded levels is used as an initial guess in the iterative scheme to derive temperature profiles from the IRIS radiances. Third, a radiosonde height provides the initial height for integrating the hydrostatic equation for IRIS derived temperatures. Fourth, the radiosonde is used for verification of the derived temperature and height profiles. A description of the data processing and the special treatment of the radiosonde and IRIS data is given in Appendix A.

The main objective of this study was to determine the temperature and horizontal geopotential height fields at stratospheric levels.

One approach to determine these parameters was to assume clouds had little or no effect on the IRIS radiances above the 100-mb level. Using the six most opaque spectral intervals of the IRIS data, temperature profiles were derived. The geopotential heights were found by integrating the hydrostatic equation using this derived temperature profile and starting with the radiosonde 100-mb height. In addition to the above approach, it seems desirable to derive the temperature profile starting at the surface to obtain heights. The surface parameters are generally defined with better resolution and are more readily available than the 100 mb data. This section treats the corrections needed for clouds, as well as for high terrain and hot terrain, and thus permitting the derivation of temperature profiles from the earth's surface.

Clouds generally exist within the field-of-view of the IRIS instrument, and hence reduce the measured radiance for the less opaque intervals that would otherwise be measured for a cloud-free atmosphere. It is necessary to correct such cloud contaminated measurements. The uncertainty of the cloud corrections is probably the single greatest source of error in the final temperatures, as the measured radiances themselves provide no information below cloud level.

To determine if a correction is necessary and then to determine the correction an independent estimate of the earth's surface temperature must be available. This temperature is taken as the shelter temperature from the radiosonde sounding and applied to each of the

IRIS sets in the interpolation group. The other quantity necessary to determine a correction is a window channel effective radiative temperature, T_e , from the average spectral radiances.

If the shelter temperature is 5°C greater than T_e , clouds are considered to exist in the field-of-view. If the shelter temperature is 5°C less than T_e , hot terrain conditions are considered to be present.

If the shelter temperature is within $\pm 5^{\circ}\text{C}$ of T_e , the atmosphere is treated as being cloud-free and no corrections are necessary, unless the location meets the high terrain qualifications. If the elevation is greater than 500 mb above sea level the clouds are assumed to reach the ground in this two-cloud level model. Hot terrain occurs when the earth's surface is much hotter than the near-surface air resulting in a much higher T_e than shelter temperature. If the IRIS radiances were left uncorrected for this hot terrain, erroneously warm temperature profiles would occur in the lower troposphere.

The corrections for clouds, high terrain and hot terrain follow very closely the technique given by Smith, et al (1970). They have developed a two-level cloud model to describe the cloud distributions from SIRS radiances and subsequently to compute radiance corrections needed to determine the temperature profile. This method can be used equally well on the IRIS data with only minor changes. For completeness, a small portion of Smith's development is repeated in Appendix B.

4.0 INTERPOLATION PROCEDURE.

This section contains a description of the procedures used to derive the temperature and geopotential height profiles from the IRIS 15-micron spectral data for locations away from the subsatellite track. A set of equivalent clear-column IRIS 15-micron radiances is determined from the original measured set for locations surrounding a radiosonde location. A regression relation is established between gradients of the MRIR 15-micron radiance and the gradients of each of the clear column IRIS radiances for all combination of locations surrounding the radiosonde. An average IRIS radiance set is found from the regression relation, distance weighted, at the radiosonde location. A temperature profile is found by the method of Section 2.3. The temperature profile is subsequently adjusted, equally at all levels, until the measured MRIR 15-micron radiance equals the computed radiance. The height profile is found by integrating the hydrostatic equation starting with the station height or 100-mb height of the radiosonde using the IRIS derived temperature profile.

The IRIS radiances, corrected for clouds, hot terrain, and high terrain were interpolated to the radiosonde locations. The computer algorithm required at least four IRIS sets for each interpolation, of which at least one set is from each of the two subsatellite tracks considered. Because the data were often noisy, the available IRIS data were reduced considerably before the interpolation was carried out. Figure 2 shows a typical case for which a set of IRIS radiances is desired at the circled dot location where only the MRIR 15-micron radiance is available, and both IRIS and MRIR 15-micron radiances at

the surrounding solid dot locations are given. The locations of the solid dots in these two nearly north-south tracks were chosen by the method discussed in Appendix A. They represent locations of the IRIS data along two successive subsatellite tracks. The circled dot location represents any arbitrary location. For operational use, using this technique, the location might be equally-spaced grid points for which temperature and height values are desired. To verify the interpolation procedure and the temperature profile derivation technique, the circled dot location was chosen here to be at the location of a radiosonde. In further discussion of this location it will be referred to as the radiosonde location, but it can be any arbitrary location within the confines of the two tracks. Along the tracks, only data which are less than 20° of latitude from the radiosonde location were used.

Eq. (1) for each of the IRIS spectral intervals and for the MRIR 15-micron channel can be written, respectively, as

$$I(\nu) = B[\nu, T_s(P_s)] \tau_s(\nu, P_s) - \int_{P_t}^{P_s} B[\nu, T(p)] \frac{\partial \tau(\nu, p)}{\partial \ln p} d\ln p \quad (4)$$

and

$$\begin{aligned} \nu_2 &= 612.5 \\ M(\nu) &= \int_{\nu_1}^{\nu_2} B[\nu, T_s(P_s)] \tau_s(\nu, P_s) \phi(\nu) d\nu \\ \nu_1 &= 717.5 \end{aligned} \quad (5)$$

$$- \int_{\nu_1}^{\nu_2} \int_{P_t}^{P_s} B[\nu, T(p)] \frac{\partial \tau(\nu, p)}{\partial \ln p} \phi(\nu) d\ln p d\nu$$

where I and M are the spectral radiances and ϕ is the filter function which is zero outside of the interval ν_1 to ν_2 .

The difference in the radiances due to the differences in the temperature profiles from one location to another, can be written

$$\Delta I(\nu) = \Delta [B(\nu, T_s) \tau_s(\nu, P_s)] - \int_{P_t}^{P_s} \Delta \left\{ B[\nu, T(p)] \frac{\partial \tau(\tau, p)}{\partial \ln p} \right\} d \ln p \quad (6)$$

and

$$\begin{aligned} \nu_2 &= 612.5 \\ \Delta M &= \int \Delta \{ B[\nu, T_s(P_s)] \tau_s(\nu, P_s) \} \phi(\nu) d\nu \\ \nu_1 &= 717.5 \end{aligned}$$

$$- \int_{\nu_1}^{\nu_2} \int \Delta \left\{ B[\nu, T(p)] \frac{\partial \tau[\nu, T(p)]}{\partial \ln p} \right\} \phi(\nu) d \ln p d\nu \quad (7)$$

Thus the changes in the radiances are due to the changes in temperature, mostly through B . Changes $\frac{\partial \tau}{\partial \ln p}$ due to the changes in the absorbing gases are negligible. For the stratosphere, this is an especially good assumption over the distances considered. Only CO_2 (always considered constant) and H_2O (which has little effect in the stratosphere) are active constituents in this spectral region.

The changes in the MRIR radiances are associated with the changes in the IRIS radiances through a scheme that will permit a set of IRIS

radiances to be specified at a location for which there is only the MRIR radiance. The following considers only one IRIS spectral interval. There are actually eleven different IRIS intervals and the same procedure applies to each. Figure 2 shows an example of a situation that can exist. The solid dots represent the locations for which both MRIR and IRIS are sampled along two successive subsatellite tracks. The circled dot represents a location for which only the MRIR exists and for which we want to determine the IRIS radiances. Separate regression analyses will be made for each point for which interpolation is desired to relate gradients of the IRIS and MRIR radiances between known points surrounding the interpolated point. The resulting regression equations will be applied to determine the change of the IRIS radiance between each known and interpolated point. The regression equations for the components of the change can be written

$$\frac{\partial I_x}{\partial x} = a_x + b_x \frac{\partial M_x}{\partial x} \quad (8)$$

and

$$\frac{\partial I_y}{\partial y} = a_y + b_y \frac{\partial M_y}{\partial y} \quad (9)$$

where I refers to the IRIS radiances

M refers to the MRIR radiances

x and y refer to the axes of a rectangular coordinate system.

The constants are determined from the normal equation of the form

$$\sum_{i=1}^n \frac{\partial I_x}{\partial x} = n a_x + b_x \sum_{i=1}^n \frac{\partial M_x}{\partial x} \quad (10)$$

and

$$\sum_{i=1}^n \frac{\partial I_x}{\partial x} \frac{\partial M_x}{\partial x} = a_x \sum_{i=1}^n \frac{\partial M_x}{\partial x} + b_x \sum_{i=1}^n \left(\frac{\partial M_x}{\partial x} \right)^2 \quad (11)$$

a similar set of normal equations apply to the y component. With these regression equation, IR , the IRIS value at the interpolated point, can be determined by

$$IR = \sum_{j=1}^n w_j \left(I_j + \left\{ \left[a_x + b_x \left(\frac{\partial MR_x}{\partial x} \right) \right]^2 + \left[a_y + b_y \left(\frac{\partial MR_y}{\partial y} \right) \right]^2 \right\}^{1/2} \right) \quad (12)$$

where w_j are the distance weights such that

$$\sum_{j=1}^m w_j = 1 \quad (13)$$

I_j are IRIS radiances at the known points. $\frac{\partial MR_x}{\partial x}$ and $\frac{\partial MR_y}{\partial y}$ are the components of the MRIR gradients between the known and interpolated points.

This scheme has the property of weighting the data nearest the interpolated point heavier than farther points and also specifies the IRIS radiances between subsatellite tracks to the degree they are accounted for by the MRIR gradients. For the less opaque spectral intervals that are weighted heavily in the lower troposphere and whose weighting curves overlap very little with the MRIR weighting curve, only a small contribution is provided in the interpolation by the correlation with MRIR gradients. In these cases the interpolation reduces to one of almost strict space weighted interpolation.

After the IRIS radiances were interpolated to the radiosonde location, a temperature profile was derived by the method of Section 2.3. Using this profile and the water vapor mixing ratio profile from the radiosonde at the interpolation point, the radiances for the MRIR 15-micron channel were computed and compared to the average observed MRIR radiance. If the two were more than 0.01×10^{-5} watt cm^{-2} steradian $^{-1}$ different, the temperature at each level was increased or decreased by 0.1C depending on the sign of the difference. This procedure was continued until the radiances agreed to within $\pm 0.01 \times 10^{-5}$ watt cm^{-2} steradian $^{-1}$.

This procedure generally required less than 10 iterations for the criteria to be met, which means that the profile based on the interpolated IRIS radiance was changed by less than 1G at all levels to get the measured and computed MRIR 15-micron radiances to agree. If the iteration repetition reached 25, the profile was eliminated from the sample.

5.0 RESULTS

5.1 Plotted Comparison of Radiosonde and IRIS Temperature Profiles

In Figures 3, 4, 5, and 6, a comparison of the IRIS derived temperature profiles with corresponding radiosonde temperature profiles is made. They were chosen to represent low, lower middle, middle and high latitude profiles. Aside from the latitude restrictions, the cases were chosen at random from the first three observation times of the period of our data sample. The solid line in Figure 3 represents the radiosonde temperature profile taken at Guantanamo, Cuba located at 19.9N, 75.2W 1200 GMT on June 16, 1969. The dashed line is the IRIS derived profile. The IRIS profile resulted from seven sets of IRIS spectral data that were interpolated to the radiosonde location. The IRIS data were recorded on two successive orbits, the subpoint tracks of which fell on both sides of the Guantanamo station. They were taken approximately 4 and 5.5 hours later than the radiosonde time. Five of the seven sets of IRIS data were corrected for low level clouds. One set, which was recorded over land, was corrected for hot terrain. The data recorded over land, during the daylight portion of orbits (near local noon), for clear skies, often require correcting for hot terrain due to the solar heating of the earth's surface resulting in a very strong lapse rate near the surface. The other set of IRIS data required no correction whatsoever. The two profiles compare fairly well; there are some differences as one would expect since the derived profile is defined for only 11 points in the atmosphere. One of the most striking features of this comparison is the accuracy with which the tropopause is defined. The choice of pressure levels used to represent the spectral

radiances of IRIS in this method of deriving profiles is, to a certain degree, arbitrary. The main consideration, of course, is that the pressure level be near the level where that particular spectral interval has a peak in its weighting function. But the levels were specified in such a manner as to improve the definition of the tropopause and other expected features of the different latitude-dependent soundings.

A better comparison of the two types of profiles is shown in Figure 4. The radiosonde profile here is for Shionomesaki, Japan taken at 1200 GMT on June 16, 1969. The tropopause is higher than on the previous sounding. The important point here, however, is that the radiance-derived sounding also specifies the tropopause quite well; although at 80 mb instead of 77 mb for the radiosonde sounding. The two soundings agree quite well, never departing more than 4°C at any height. The IRIS sounding was derived using four cloudy IRIS radiance sets taken at night on the southbound portion of the orbit approximately 2 and 3.5 hours after the radiosonde time.

Figure 5 shows the comparison of the Maniwaki, Quebec sounding taken at 1200 GMT on June 16, 1969 and the corresponding IRIS temperature profile. This case is typical of a middle latitude, summer hemisphere temperature distribution. Contrary to the two previous samples, this one does not have a very well defined tropopause, yet the two soundings compare very favorably throughout the atmospheric depth of interest, never departing by more than 4°C at any level. It should be pointed out that the IRIS sounding will not define the small perturbations that show in the Radiosonde sounding (e.g., the isothermal layer from 35 to 25 mb) because the technique defines temperatures only at predetermined levels.

The IRIS profile was derived from a set of data interpolated from seven surrounding IRIS radiance sets. In this case there were high clouds along the subsatellite track to the east of Maniwaki, and to the west there were hot terrain conditions. Corrections were applied accordingly. The IRIS data were recorded approximately 4 and 5.5 hours later than the radiosonde data on two northbound orbits at near local noon.

The comparison of the radiosonde and the IRIS temperature profiles in Figure 6 is not as good, at least below the tropopause, as in the previous examples. Above 200 mb, however, the two profiles agree very well.

5.2 Verification Statistics

The ultimate test of any new method is to compare the results with those of some accepted standard. Figure 7 depicts the variation of the RMS difference between the radiosonde and the interpolated, IRIS-derived temperature for five latitude bands. The RMS differences were calculated and plotted at the 15 mandatory pressure levels from 1000 to 10 mb. It can be seen that the differences are much greater in the troposphere than in the stratosphere. Except at 20 mb in the tropics, the RMS differences in the stratosphere are generally between 2C and 5C. The 10 and 20-mb RMS differences for the tropical case were based on only 7 and 23 cases, respectively, and are, therefore, probably unreliable. Except, again, for the tropical and arctic cases, the RMS differences are less than 5C for the troposphere above 300 mb. There are large RMS differences at 400 mb for all but the high latitude case and at 1000 mb for all but the tropical case.

When the sign of the difference (radiosonde minus IRIS) at these two levels is considered (Figure 8), it is found that at the 1000-mb level, the IRIS temperature is practically always warmer than the radiosonde. On the other hand, the radiosonde is always warmer than the IRIS temperature at 400 mb. Of course, the reason for the reduction in the RMS difference near 700 mb is due to this change in sign and to the fact that IRIS temperatures are determined only at these two levels and interpolated in between. There are two possible reasons for the cooler IRIS temperatures at 400 mb. First of all, the pressure adjustment factor used to improve the transmittance values, may still be underestimated for the spectral interval corresponding to the 400 mb level. This underestimation would result in computed temperature values being too low. Second, the correction technique for the cloud contaminated radiances results generally in too low temperature values. Probably both of these causes contribute to the low IRIS temperature.

On the other hand, the high 1000-mb temperature can not be explained by the cloud correction method, although an erroneous pressure correction has probably resulted in an overestimation of the temperatures at this spectral interval. Another factor that may contribute to the overestimation of the 1000 mb temperature is the method used to specify the surface for cloud correction cases. The surface (shelter) temperature of the radiosonde was used to specify the surface temperature for all surrounding IRIS sets. A method that might improve the specification of the surface temperature is one that interpolates the horizontal surface temperature field using all available surface information for the most recent observation time, and then to specify the diurnal temperature change since the observation time.

Figure 9a and 9b show the RMS difference (radiosonde minus IRIS) in the geopotential height field. Figure 9b is based on the integration of the hydrostatic equation using IRIS temperature starting with the 100-mb radiosonde height. The RMS differences for stratospheric levels are from about 100 to 300 meters in (a) but are only 20 to 160 meters in (b). In Figure 10a and 10b the average height differences are plotted for each of the latitude bands. In Figure 10a the tropical curve extends beyond the limit of the graph between about 300 and 180 mb with a maximum of 194 meters at 250 mb and again above 25 mb with a maximum difference of 250 meters at 10 mb. In both Figure 9 and 10 it is apparent that cumulative differences occur due to the integration. Therefore, the differences are much smaller in the stratosphere when the integration is started at 100 mb than when the integration is begun at the surface. Because the geostrophic wind is dependent upon the horizontal gradient of the height field and not upon the absolute value of height at any level, the cumulative errors of height might be less significant than those of temperature when estimating winds. The horizontal gradients of heights are compared in the next section in the form of maps.

Table 1 shows the correlations level by level between the radiosonde and IRIS derived temperature profile. The correlation coefficients for the individual latitude bands are less than the corresponding coefficients when all latitudes are included in single data sample. This is because the average large-scale temperature change from the pole to the equator is well correlated, but the much smaller variability within any one latitude band is much less correlated. The IRIS measurements and the

temperature reduction technique cannot specify the small-scale vertical temperature changes that are shown in the radiosonde profiles, although the large-scale temperature changes are quite well determined. Because the IRIS measurements were smoothed due to noise and because the reduction technique specifies temperatures at only 11 pressure levels and intermediate levels are interpolated, it is not expected that the small-scale changes in the vertical will be specified as well in the IRIS as in the radiosonde temperatures.

Table 2 shows the correlation of heights for both the surface integration and the 100-mb integration of the hydrostatic equation. The correlation of the heights at levels above 100 mb is naturally much improved when the integration starts at 100 mb, rather than at the surface. The RMS difference (Figure 7) and the absolute difference (Figure 8) of temperature show a minimum at 100 to 70 mb for all latitudes. The correlations (Table 1) are greatest, as well, at these levels. These facts are significant because the MRIR 15-micron weighting curve (Figure 1) shows a maximum near these levels, indicating that the interpolation is best at those levels that contribute the most to the measured MRIR radiances.

Because there is a systematic difference in the IRIS derived and the radiosonde temperatures, the interpolation method may be improved by eliminating this difference. The improvement can be made by finding the cause for the difference and correcting it, or for any data set, simply subtracting the mean of the absolute difference from the derived temperature at any level. For example, at 400 mb (a level for which temperature is derived from the IRIS interpolated data) for the 0-22.5° latitude case, the RMS difference can be reduced to 4.1K by subtracting

the square of the absolute difference, 64.0° (Figure 8) from the square of the RMS difference, 81.0° (Figure 7) and taking the square root. The improvement is from 9.0K to 4.1K.

5.3 Comparison with NMC Analysis

An area with good satellite data coverage and a time which had relatively moderate horizontal temperature and height gradients was selected to show the operational potential of the technique to improve the description of these variables between subsatellite tracks in the stratosphere. The area chosen was 50W to 30E, and 40 to 68N, so as to have the least time difference with the 1200Z NMC map which was used for comparison. Data from orbits 913, 914, and 915 on June 21, 1969 were used to construct the IRIS maps. The data from orbit 913 over this area was recorded from approximately 0943 to 0952, orbit 914 from 1130 to 1139, and orbit 915 from 1317 to 1324 GMT. Thus the data to the east of Greenwich was taken slightly more than 2 hours before the radiosonde data, the satellite data near and just to the west of 0° was taken just prior to the radiosonde, and the data over the western portion was taken more than an hour after the radiosonde.

For this application, no use whatsoever was made of radiosonde data except to specify the 100-mb height field for determining, hydrostatically, the heights of higher levels. Because only stratospheric levels were used, surface temperature was not needed and water vapor was specified from climatology. The iteration to derive temperature profiles was initiated by using an isothermal profile of 250K. Temperature and height profiles were computed at each intersection of a 4° longitude by 4° latitude grid for which radiation data existed over this area.

Figure 11 is a portion of the NMC 100-mb map for this area showing the temperature and height field. The orbital tracks along which

IRIS data were observed, on this and subsequent maps are shown for reference. The height field from this map was used to determine higher level heights from the IRIS temperature profiles. The temperature field shows a warm center near 10°W, 55°N and with a relatively large thermal gradient (for a summer map) over the southwest region. Figure 12 shows the interpolated IRIS temperature field at the same 100-mb level. The warm center and the strong gradient are both well defined; in fact, both the pattern and absolute values of the isotherms are in good agreement with the NMC analysis over the entire map. It is interesting to note that the interpolated IRIS data reveals the eastern extreme of the warm -50C center in complete agreement with the dense western European radiosonde data. Had only subsatellite radiation data been available, this would probably not have been shown as far to the east. However, over an area for which no radiosonde data were available, the IRIS interpolation indicates a warm trough in the -55C isotherm along 20W, not shown in the NMC analysis, yet in agreement with the NMC trough in the -65C isotherm at 33W and 33N (beyond the border of the reproduced map).

Figures 13 and 14 show respectively, the NMC and the IRIS temperature and height analysis for 50 mb. The warm trough in both figures is in good agreement, although the IRIS -50C trough is about 10° east of the NMC trough. The NMC position is well supported by the available but sparse ocean station data, so the difference is not readily explainable. The IRIS map defines the feature quite well and the magnitudes of the isotherms agree well. The northward bending of the -55C IRIS isotherm at 20E is not shown by the NMC

analysis, but can be justified by the radiosonde data. The difference in analysis here can be attributed to the greater smoothing of the NMC procedures. It is interesting that the radiation data supported an analysis which the conventional technique ignored. Again, if only spatial interpolation from one subsatellite track to the next was used, this feature would have been missing on the IRIS analysis also. The IRIS map does not show the -45C isotherm that appears on the northern boundary of the NMC map because of the lack of radiation data here on this day. The temperature fields in Figure 15 and 16 for the 10-mb level do not compare as favorably as on the 50-mb map. The NMC map shows a warm tongue of -30C farther west than the IRIS map. The NMC -40C cold center along 5W does not appear on the IRIS map. Inspection of the radiosonde data shows wildly different temperatures in this area, such as -26C adjoining -43C. The IRIS analysis appears as justified as the NMC in this instance considering the number and variance of the few reports available on this map. The IRIS map also shows much more detail than the NMC map.

The NMC automatic analysis employs extensive smoothing with an initial scan over 5 NMC grid points, even where data are plentiful. Also over this part of the ocean where there may be only 2 or 3 radiosonde stations, it may not be possible for the NMC analysis to detect such small scale features as the low center at 30W on the IRIS map at 50 mb. Another factor contributing to the uncertainties, especially at 10 mb, is that radiosonde data are extrapolated vertically when they do not reach these levels. In addition, it is not uncommon for heights at 10 mb to differ by 100 meters and sometimes even 200 meters between neighboring stations only a few

hundred kilometers apart. The standard deviations determined from the radiosonde data used in Section 5.3 for heights at 50 and 10 mb are 121 and 258 meters, respectively, while for the IRIS heights, the standard deviations were 105 and 270 meters, respectively. Although the agreement at 50 and 10 mb in the height field is not good, the uncertainties in the IRIS values are probably no greater than those of the radiosondes at these levels.

Hence it appears possible that the interpolated radiation data can provide more detailed, and as reliable, information as can be estimated from NMC data. It is paradoxical, however, that the thermal fields from independent data appear to agree better than the height fields which are based on a common 100-mb base.

5.4 Sources of Error

There are many factors that contribute to errors and uncertainties in the temperature and geopotential height profiles derived by the procedures used in this study. Some of them are:

1. Foremost, perhaps, are the errors introduced when clouds contaminate the radiances. These errors are certainly more severe in the troposphere than in the stratosphere because of their more frequent occurrence in the lower atmosphere. Clouds may have, however, a significant effect on the stratospheric temperatures and heights derived from the 100 mb level in cases when these clouds penetrate to high levels. The MRIR 15-micron data were not corrected in any way for cloud effects on the assumption that only very high clouds would result in significant errors and the averaging of these data would tend to smooth the few affected radiances.
2. The noisy IRIS data could also contribute to the errors, although, severe smoothing was applied to eliminate extremes from occurring. However, this process also eliminated any large, true signals.
3. Time differences (up to \pm 6 hours) between the observations of radiosonde and radiation data. Some of these uncertainties are due to the actual physical differences in the atmosphere in time. Time and space differences also introduce errors in the method used to specify the surface temperature, and the subsequent correction for cloud contaminated IRIS radiances.
4. The many approximations in the solution of the radiative transfer equation and the iterative technique to derive temperature

profiles. Especially contributory to the errors is the uncertainty in the absorption coefficient of CO₂ for the 15-micron band. The specification of the anchor pressure bands in the temperature profile derivation technique is a possible source of error. Definitely, the interpolation between anchor levels adds to the errors.

6. The interpolation technique to specify IRIS profiles between tracks is based on regression, and statistical errors can occur due to inadequate sample size.

7. Uncertainties can occur due to errors in the radiosonde temperatures themselves.

6.0 SUMMARY AND CONCLUSIONS

To improve the specification of stratospheric horizontal temperature and geopotential height field from satellite radiation data, a technique has been derived to estimate vertical pressure-temperature-height profiles between subsatellite tracks using interpolated IRIS 15-micron data. The interpolation is based on the linear regression of the IRIS and MRIR 15-micron radiance gradients between points along the tracks for which both are available. The regression equation is then applied to locations away from the track where only the MRIR exist. A set of IRIS 15-micron radiances is specified by the interpolation. In the interpolation each set of IRIS radiances is corrected for clouds and hot terrain. A temperature-pressure profile is derived from the radiances using an iterative technique. The temperature profile is adjusted equally at all levels, until the MRIR 15-micron radiance computed from the profile equals the measured MRIR radiance at the same location. Using this derived temperature profile, the hydrostatic equation is integrated to find geopotential heights. The integration was done starting at both the surface and a known 100 mb radiosonde height.

This technique was verified by interpolating to radiosonde locations and ignoring up to 6 hours time difference between radiosonde and radiation observations. The sample varied from 1126 pairs at lower levels to 383 pairs at 10 mb using northern hemisphere data for June 15 to July 20, 1969. The data were also separated into 5 latitude bands and separate analysis done for each band.

The RMS differences of the radiosonde and IRIS derived temperatures were generally between 2 and 5C for all levels above 300 mb.

For levels below 300 mb, the RMS difference was as high as 9.5C at 1000 mb for the high latitude case. The IRIS temperature was consistently warmer than the radiosonde at 1000 mb but colder at 400 mb. Generally, the radiosonde temperatures are warmer than the IRIS temperatures above 100 mb. At 50 mb the radiosonde temperature is approximately 2C warmer for all latitudes. The difference decreases upward and for high latitude cases the IRIS temperature is nearly 4C warmer than the radiosonde at 10 mb.

The RMS difference of the radiosonde and IRIS heights ranges from 30 to 280 meters, generally increasing from the surface to 10 mb when the hydrostatic equation was integrated from the surface to 10 mb. Starting the integration at 100 mb, above the cloud level, resulted in far lower RMS differences, ranging from 20 to 120 meters from 70 to 10 mb.

The horizontal gradients of temperature derived by this method compared favorably with the gradients from NMC computer analysis for a limited area at the 100, 50, and 10-mb levels. The strict spatial interpolation between tracks of the IRIS temperatures resulted in the loss of considerable detail. In the limited comparison, the height fields derived from the IRIS temperature profiles probably have no more uncertainty than the radiosonde heights at those levels.

It can be concluded from this study that the interpolated IRIS derived temperature and height profiles can be determined accurately enough to improve the temperature gradients between tracks for stratospheric levels. Such improvements in gradients are of significant practical importance to high-flying aircraft. This technique can thus be a useful operational tool, although it could benefit from an improved understanding of all the error sources.

Several recommended areas of investigation may improve the results of using this technique. First, the specification of the height field might be improved by using a statistical method of deriving the heights instead of relying on the integration of the hydrostatic equation. In this method a regression relation is established between IRIS radiances and the heights from radiosondes. The regression equation is then applied to the interpolated IRIS radiances to get heights. This method has worked successfully for tropospheric levels using Satellite Infrared Spectrometer (SIRS) radiation data (Smith, et al, 1970).

Second, a more detailed study is recommended to find improved CO₂ transmission coefficients and pressure correction factors to improve the transmission values used in the solution of the radiative transfer equation. Third, improvements may possibly be made in the specification of the anchor pressure levels needed in the temperature profile derivation scheme.

Fourth, an improved data set may also improve the results. In this study it was necessary to use noisy IRIS data for the summer stratosphere. Using noise-free, winter, stratospheric data which has far greater horizontal temperature and height gradients may improve the results.

7.0 REFERENCES

- Barnett, Thomas L., 1969: Application of a nonlinear least-squares method to atmospheric temperature sounding. J. Atmos. Sci., 26, 457-461.
- Chahine, M.T., 1968: Determination of the temperature profile in a atmosphere from its outgoing radiance. J. Opt. Soc. Amer., 58, 1634-1637.
- Chahine, M.T., 1970: Inverse problems in radiative transfer: determination of atmospheric parameters. J. Atmos. Sci., 27, 960-967.
- Conrath, B. J., R. A. Hanel, V. G. Kunde, and C. Prabhakara, 1970: The infrared interferometer experiment on Nimbus 3. J. Geophys. Res., 75, 5831-5857.
- Hanel, R., B. Schlachman, F. D. Clark, C. H. Prokesh, J. B. Taylor, W. M. Nelson and L. Chaney, 1970: The Nimbus 3 Michelson interferometer. Appl. Opt., 9, 1767-1775.
- Kaplan, L. D., 1959: Inference of atmospheric structure from remote radiation measurements. J. Opt. Soc. Amer., 49, 1004-1007.
- King, J.I.F., 1958: The radiative heat transfer of plant earth, in Scientific Uses of Earth Satellites, 2nd ed., edited by J. A. Van Allen, University of Michigan Press, 316 pp.
- King, J.I.F., 1964: Inversion by slabs of varying thickness, J. Atmos. Sci., 21, 324-330.
- Rodgers, C.O., 1966: Satellite infrared radiometer; A discussion of inversion methods. Univ. of Oxford Clarendon Lab. Mem. 66.13, 25 pp.

- Smith, W. L., 1966: Note on the relationship between total precipitable water and surface dew point. J. Appl. Meteor., 5, 726-727.
- Smith, W. L., 1969: A polynomial representation of carbon dioxide and water vapor transmission. ESSA Technical Report-47, U.S. Department of Commerce, National Environmental Satellite Center, Washington, D.C., 20pp.
- Smith, W.L., 1970: Iterative solution of the radiative transfer equation for temperature and absorbing gas profiles of an atmosphere. Appl. Opt., 9, 1993-1999.
- Smith, W. L., H.M. Wolf, W.J. Jacob, 1970: A regression method for obtaining real-time temperature and geopotential height profiles from satellite spectrometer measurements and its application to Nimbus 3 "SIRS" observations. Mon. Wea. Rev., 98, 582-603.
- Strand, O.N., and E.R. Westwater, 1968: Minimum RMS estimation of the numerical solution of a Fredholm integral equation of the first kind. SIAMJ. Numer. Anal., 5, 287-292.
- U. S. Standard Atmosphere Supplement, 1966: Prepared under sponsorship of ESSA, NASA, U.S. Air Force. Available from the Superintendent of Documents, U.S. Government Printing Office, Washington, D.C., 20402, 289pp.
- Wark, D. Q., and H. E. Fleming, 1966: Indirect measurements of atmospheric temperature profiles from satellites, 1, introduction. Mon. Wea. Rev., 94, 351-362.

APPENDIX A

Data Processing

This appendix treats in detail the processing of each of the three sets of data used in this study. The final location in space and time of all three sets for the interpolation of the IRIS radiances to radiosonde locations for verification is also described.

A.1.0 Radiosondes

The radiosonde soundings were taken from the National Meteorological Center Automatic Data Processing (NMC ADP) file data supplied by the National Climatic Center, Asheville, North Carolina. Each tape reel had seven days of data for each of the 00Z and 12Z observations times. Packed binary records contain various types of observations - radiosondes, pibals, ship reports, aireps, and even some temperature profiles generated from the Nimbus III SIRS data. The NMC data were subjected to a preprocessing before being merged with the radiation data. Only land and ship radiosondes were unpacked and converted to CDC-6600 60-bit binary format. In addition, soundings with location errors and ones that didn't extend to 70 mb were not converted. Approximately 400 of the original 1800 to 2000 observations per observation time remained. By preprocessing the NMC tapes, the input time was reduced by a factor of 10 when the actual merging of the three sets of data was done. At that time the NMC data were transferred from the preprocessed tape to Extended Core Storage, ECS, one day at a time.

After the location of all three sets of data, the soundings were further tested and defined from the surface to 0.1 mb. The mixing ratio of water vapor was computed from the dew point temperature using the Clausius-Clapeyron equation to find the vapor pressure, e, and the mixing ratio, W, was defined by

$$W = .622 e/p 10^3 \quad (1)$$

at pressure, p.

The Northern Hemisphere was divided into five latitude zones, 0-22.5°, 22.5-37.5°, 37.5-52.5°, 52.5-67.5°, and 67.5-90°. These zones correspond to the 5 standard atmospheres for July found in the U.S. Standard Atmosphere Supplement, 1966. Each radiosonde temperature profile was extrapolated from its highest level to 0.1 mb by one of the five standard atmospheres depending on the latitude zone in which the sounding was located. The mixing ratio was extrapolated by

$$W = W_L \left(\frac{P}{P_L} \right)^\lambda \quad (2)$$

where W_L is the mixing ratio of the next lower pressure level, P is the pressure of the level for which the mixing ratio is to be defined,

P_L is the pressure of the next lower level,

λ is a climatological value given by Smith (1966). For this report λ takes values according to the 5 latitude bands for summer of 2.75, 2.96, 2.77, 2.62, and 2.10.

The mixing ratio was extrapolated to the tropopause in this manner. If the mixing ratio at the tropopause was less than 0.002 g kg^{-1} , it was extrapolated to 0.1 mb at that value. If the mixing ratio was greater than 0.002 g kg^{-1} , it was set equal to 0.002 for every element of the array up to 0.1 mb. Checks were made to determine that all elements of the radiosonde sounding were defined and reasonably accurate. If temperatures were found undefined or unreasonable, all elements at the same level were eliminated. However, if the temperature element was accepted and the dew point temperature unacceptable, the dew point value was found by interpolating from higher and lower level values. Heights were found by hydrostatic integration. At this point in the data processing, the radiosonde matrix of pressure, height, temperature, and mixing ratio was complete for all pressure levels for which a temperature element existed after the checking procedure, including significant levels of the extrapolated temperature and mixing ratio curves to 0.1 mb.

A.2.0 IRIS data

The IRIS data were provided by the National Space Science Data Center , NSSDC. Approximately two reels of tape contain data for one day in CDC-6600 binary format. Only portions of the atmospheric spectra (Record Type 8; See Nimbus III Users' Guide) plus location information were processed. The data stored in ECS were contained in 130 words consisting of the radiances for the water vapor, CO₂ 15-micron, and the 11-micron window portions of the spectrum; however, the water vapor data were not used. There were at most 5400 spectra available per day.

Unfortunately, the IRIS spectral data were noisy for the period used in this work. No attempt was made to use only the relatively good data, such as data acquired on northbound portions of orbits before playback. The IRIS data were smoothed spectrally and averaged spatially during the interpolation process. In addition, if after smoothing and averaging, the number of iterations required to converge the temperature profile to the prespecified value was greater than ten, the data were considered too noisy and this data group was eliminated from the sample. The spectral smoothing of the radiance was accomplished by using a four-point linear interpolation scheme to interpolate for the needed wave numbers from the wave numbers recorded for the IRIS spectrum.

The same set of cloud-free IRIS data used to determine the adjustments for the CO₂ transmissions (Sec. 2.1) was also used to eliminate excessively noisy data. The IRIS cloud-free data were grouped into one of five latitude bands for the northern hemisphere and averages determined for each band. During the processing of the data each IRIS radiance value was compared to its corresponding latitude average. If the average radiance for any of the six uppermost channels, was more than 3.0×10^{-5} watt cm⁻¹ steradian⁻¹ from the average, the entire set was eliminated from the sample, as being too noisy, although cloudiness may also have been a factor.

A.3.0 MRIR Data

The MRIR data were also supplied by NSSDC. One reel of tape contained approximately one day of data in 36-bit binary format.

Although data from three of the five channels were read, only the 15-micron channel data were utilized in this study. The data were stored on a disk file which can be randomly accessed. The disk was used because the 500,000 60-bit ECS words were filled with NMC and IRIS data. There were at most 11,520 swaths per day containing about 81 scan spots. During the merging process, data spots with nadir angles greater than 45°, data flagged as zero or missing, and duplicated data were discarded.

A.4.0 Processing to Locate Corresponding Data Sets

All three types of data had gaps of one kind or another. The radiosondes are not always reported, and some are not usable. Entire orbits of the radiation data are often not read out, and often the sensors are not programmed to record. They never record during playback. A search-sort-merge process is required to find corresponding data in space and time. All three types of data for one day are stored in the computer for the sort-search-merge process to begin.

The IRIS data along the 15-micron MRIR data are used to generate temperature and subsequent height profiles. The preliminary data processing is a merging operation to find a group of suitable IRIS and MRIR 15-micron data for each available radiosonde. The following sequence of operations is used to match the three corresponding sets of data in space and time; and thus, to set up data groups for which the IRIS data can be interpolated to the radiosonde locations. The processing is done one day at a time.

1. Read one radiosonde sounding from ECS.
2. A circle of sufficient radius surrounding the radiosonde location is divided into 16 equal sectors. All IRIS spectra located within 6 hours of the radiosonde time are searched within a sector. If more than one is found, the one nearest in space to the radiosonde is retained. All IRIS points, however, must be within a distance equal to 20° of latitude. At least 4 IRIS spectra are required to do interpolations. If four are not found, control goes to the next radiosonde.

3. A search is made for all MRIR data on the disk within 6 hours of the radiosonde time and within 0.65° of latitude and 0.65° of longitude/cos(latitude) of the radiosonde location. If no MRIR data are available, the next radiosonde is processed.
 4. For each IRIS spectrum, a search is made for all of the MRIR data within 6 hours of the spectrum time and within 0.65° of latitude and 0.65° of longitude/cos(latitude).
 5. If all matching requirements are met, the data are written onto tape for further processing.
 6. Steps 1 through 5 are repeated for each radiosonde sounding.
- The radiosonde and its corresponding IRIS and MRIR data is referred to as an interpolation group. Each of the 35 days of data is processed in turn. The 23 input tapes per week - 2 NMC, 15 IRIS, and 7 MRIR were finally condensed into one output tape.

APPENDIX B

Corrections for Clouds and Hot Terrain

The radiances measured from an atmosphere containing no more than two levels of clouds can be given by

$$I\nu = B[\nu, T(P_s)] \tau(\nu, P_s) - \int_0^{P_s} B[\nu, T(p)] d\tau(\nu, p) \quad (1)$$

$$\begin{aligned} & -A_U \{ B[\nu, T(P_s)] \tau(\nu, P_s) - B[\nu, T(P_U)] \tau(\nu, P_U) \\ & - \int_{P_U}^{P_L} B[\nu, T(p)] d\tau(\nu, p) \} - A_L (1 - A_U) \{ B[\nu, T(P_s)] \tau(\nu, P_s) \\ & - B[\nu, T(P_L)] \tau(\nu, P_L) - \int_{P_L}^{P_g} B[\nu, T(p)] d\tau(\nu, p) \} \end{aligned}$$

The subscripts U, L refer to the upper and lower level clouds, s refers to a surface (cloud or ground) and g is the ground.

The correction which is to be added to the measured radiances to give the equivalent clear column radiances is defined by

$$C(\nu) = A_U X[\nu, P_U, P_L, T(p)] + A^* Y[\nu, P_L, T(p)] \quad (2)$$

where X and Y are the first and second terms in brackets of Eq. (1), and $A^* = A_L (1 - A_U)$. In computing C, clouds are allowed to exist at any two-level combination of the standard pressure levels below 150 mb. Given an estimate of the temperature profile, estimates of the equivalent clear column radiances for the three spectral intervals (712.5, 757.7, 899.0 cm^{-1}) most sensitive to clouds are computed using Eq. (1).

A correction is given by

$$\hat{C}(\nu) = \hat{I}_c(\nu) - I(\nu) \quad \nu = 712.5, 757.5, 899 \text{ cm}^{-1} \quad (3)$$

I_c is the clear column radiance from Eq. (1) of Section 2.1 and I is the measured radiance. Values of X and Y are calculated for all combinations of upper and lower level cloud pressures using the estimated profiles. A_U and A^* for all upper and lower level clouds are found from Eq. (2) for the spectral intervals 712.5 and 899 cm^{-1} when \hat{C} from Eq. (3) is substituted for C in Eq. (2).

The most probable upper and lower level cloud condition is then determined from the 757.5 cm^{-1} spectral interval, the most probable cloud condition is specified as that for which $|C(\nu) - \hat{C}(\nu)|$ is a minimum. With these values of the cloud condition, the clear column radiances for the remaining spectral intervals can be calculated.

The initial temperature profile is determined from the six most opaque spectral intervals used in this study and the surface (shelter) temperature. The six opaque radiances define the temperature profile from about 10 to 100 mb. Levels between 100 mb and the surface are found by interpolation. Improved estimates of the radiances are used to estimate another temperature profile from which further cloud corrections are obtained. This iteration is continued until the change in the equivalent clear column radiances is less than a small predetermined amount. This set of radiances is thereafter treated the same as clear column radiances in the interpolation scheme.

The correction for hot terrain is obtained by

$$K(\nu) = \{B(\nu, T_{sh}) - B(\nu, T_g)\} \tau(\nu, P_s) \quad (4)$$

T_{sh} is the shelter temperature and T_g is the window channel radiative temperature. $K(\nu)$ is determined for each spectral interval and subtracted from the measured radiance for that spectral interval.

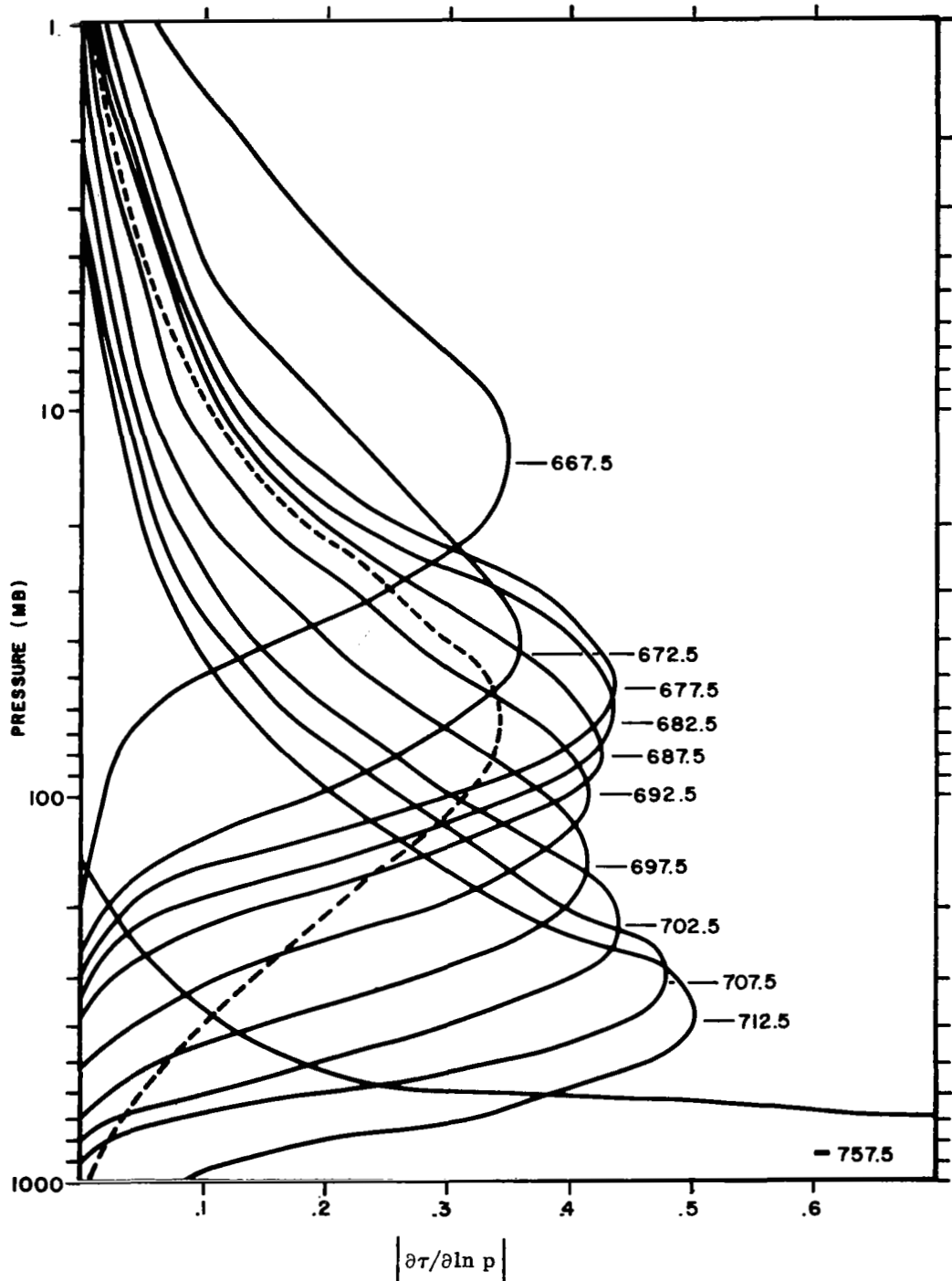


Figure 1. Atmospheric weighting functions for the 667 cm^{-1} carbon dioxide absorption band. The 757.5 cm^{-1} weighting curve peaks at 1000 mb at 1.3. The MRIR 15-micron channel ($645\text{-}690 \text{ cm}^{-1}$) is also shown (dashed line) for comparison.

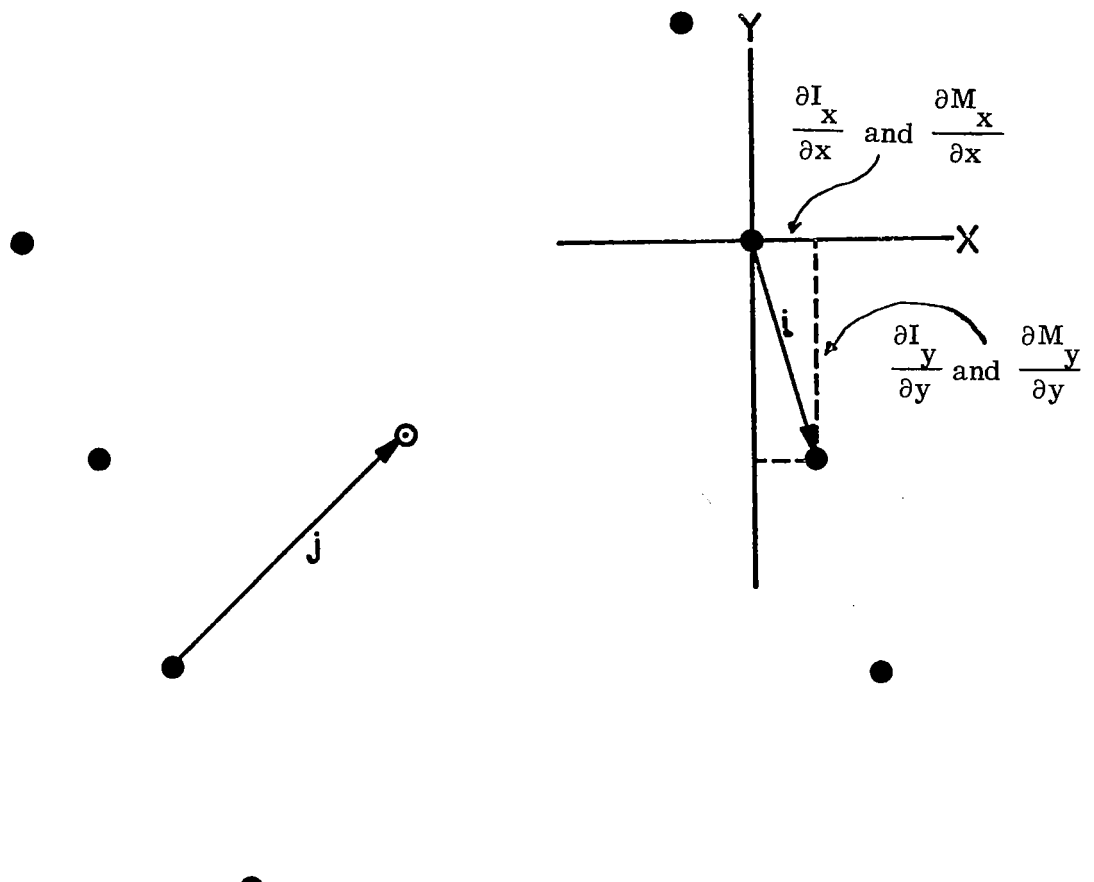


Figure 2. An example of the Interpolation Scheme. The solid dots represent points for which both IRIS and MRIR exist. The change between these points is indicated by the subscript i. The circled dot is the location for which only MRIR is known and for which the interpolation of the surrounding IRIS is desired. Change from the known to the interpolated point is marked by a subscript j.

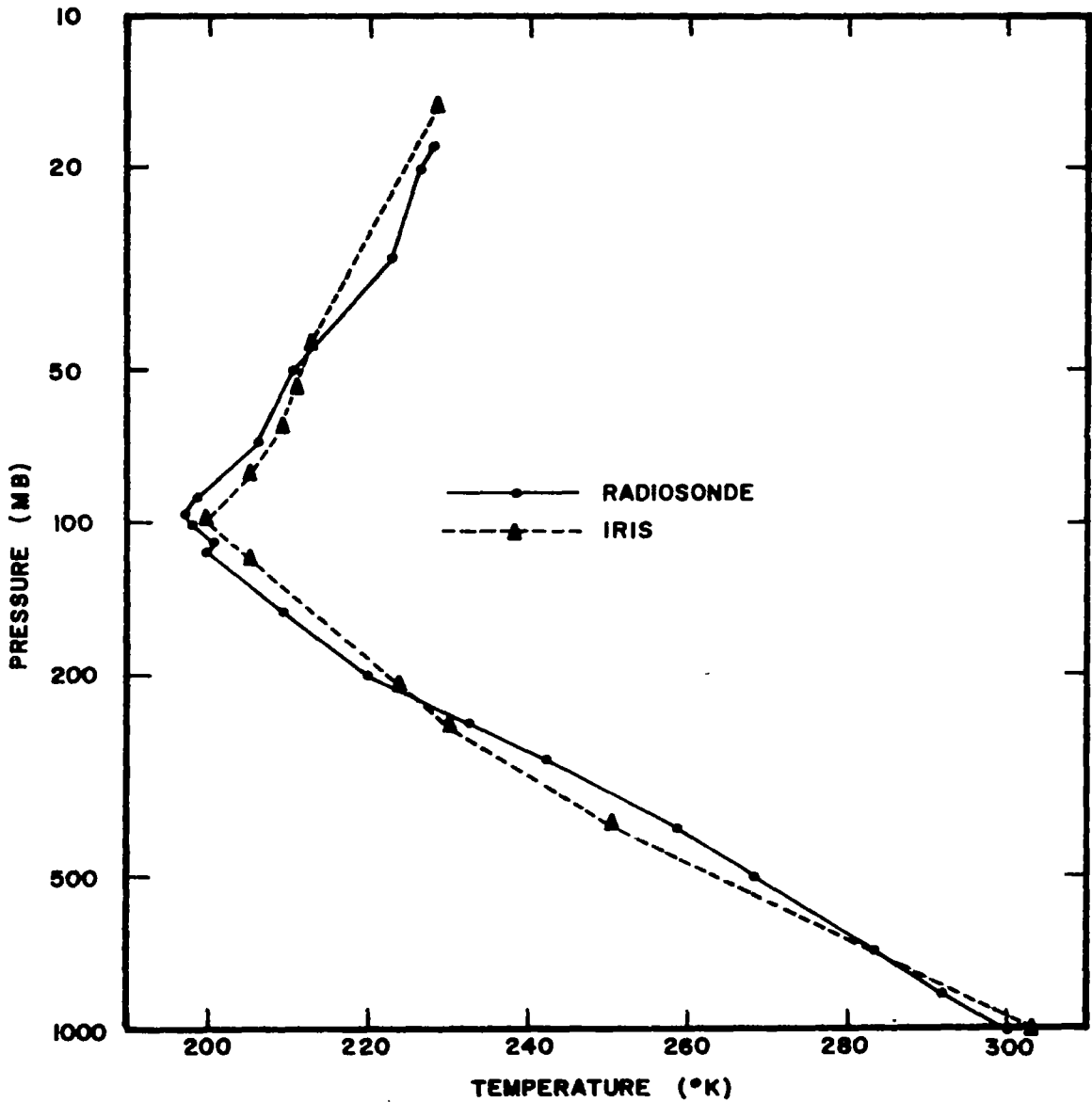


Figure 3. Comparison of a low latitude, interpolated IRIS-computed temperature profile with a radiosonde sounding over Guantanamo, Cuba, 1200 GMT, June 16, 1969.

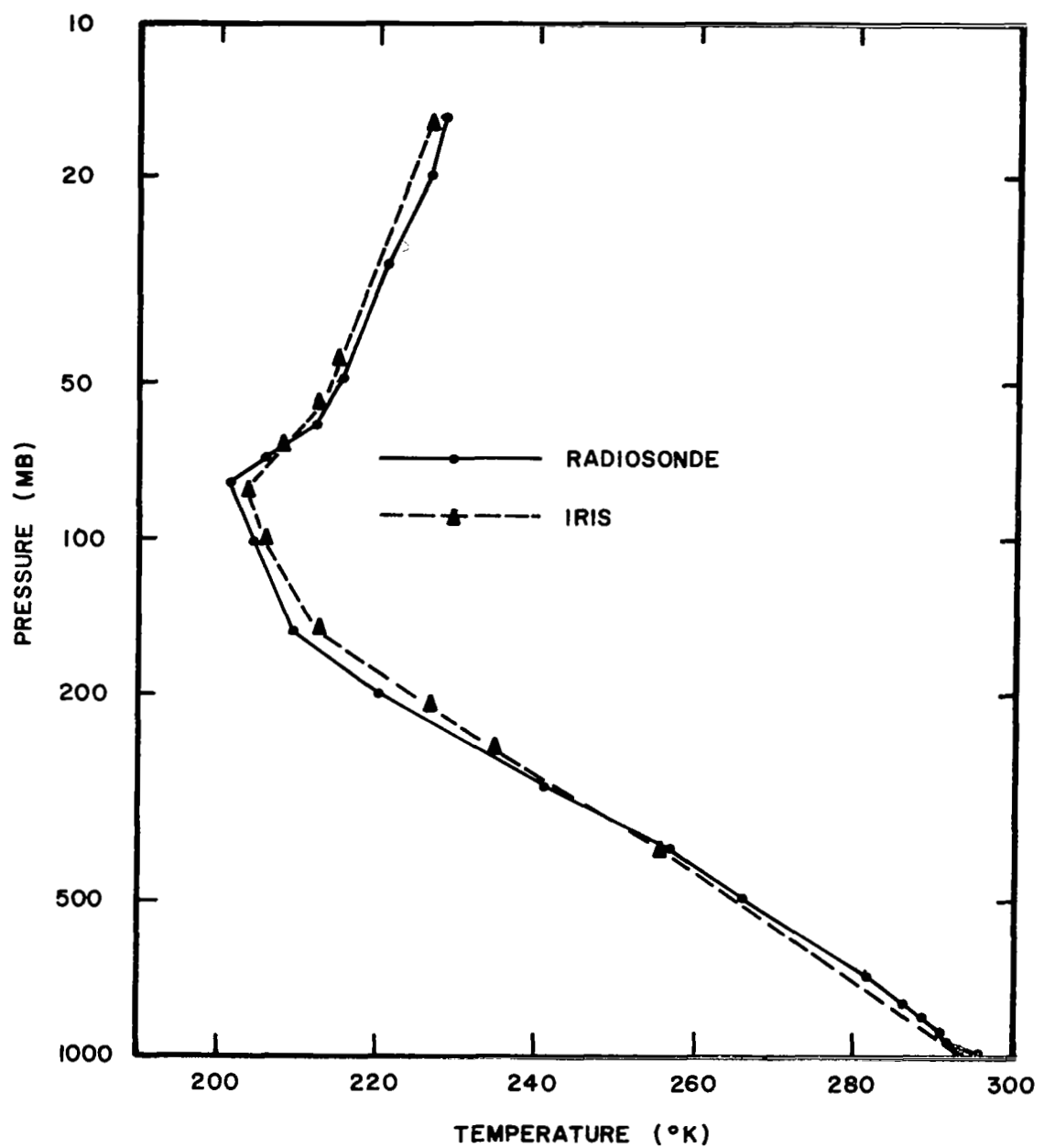


Figure 4. Comparison of a lower-middle latitude, interpolated IRIS-computed temperature profile with a radiosonde sounding over Shionomisaki, Japan, 1200 GMT, June 16, 1969.

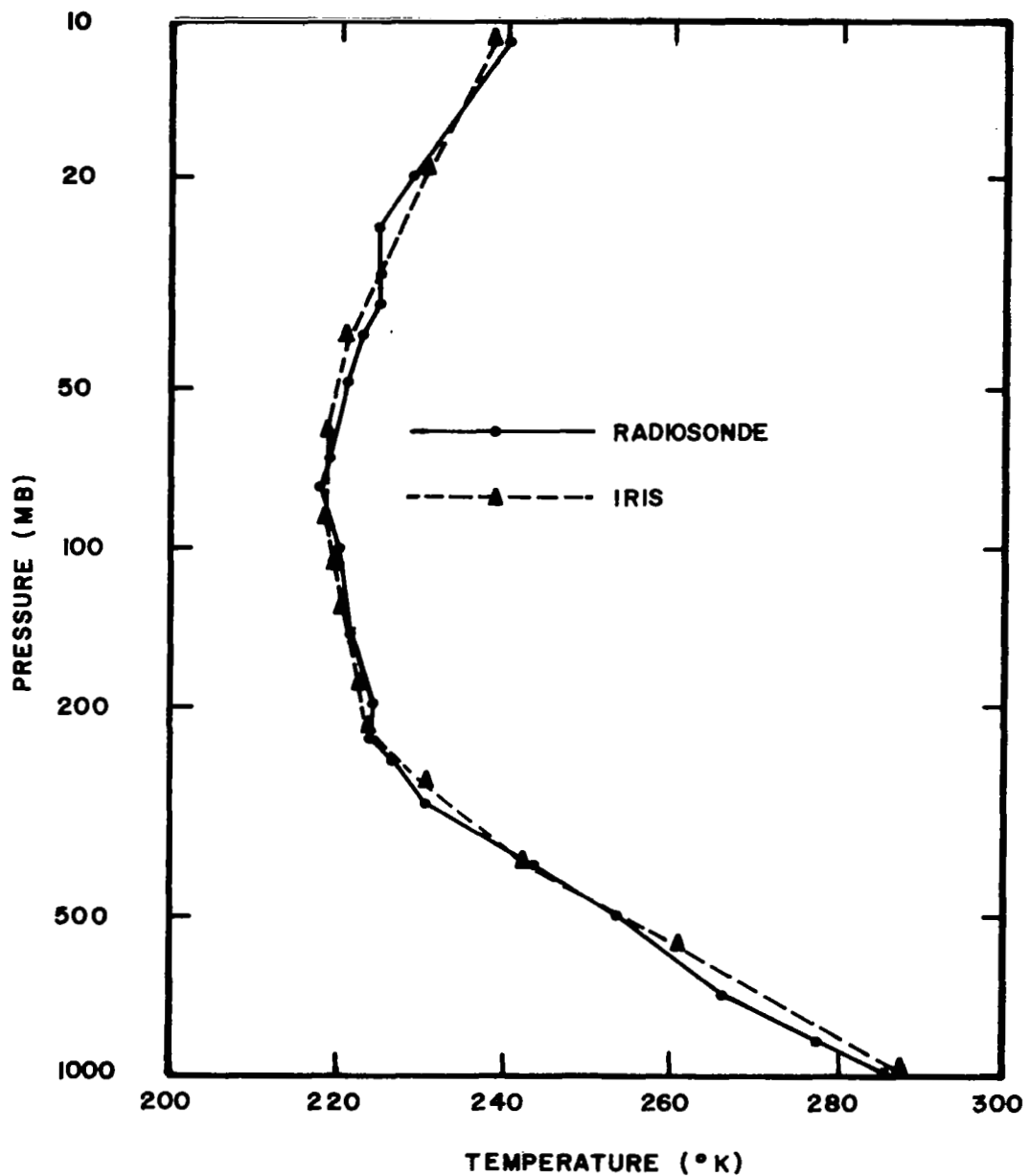


Figure 5. Comparison of a higher-middle latitude interpolated IRIS-computed temperature profile with a radiosonde sounding over Maniwaki, Quebec taken at 1200 GMT on June 16, 1969.

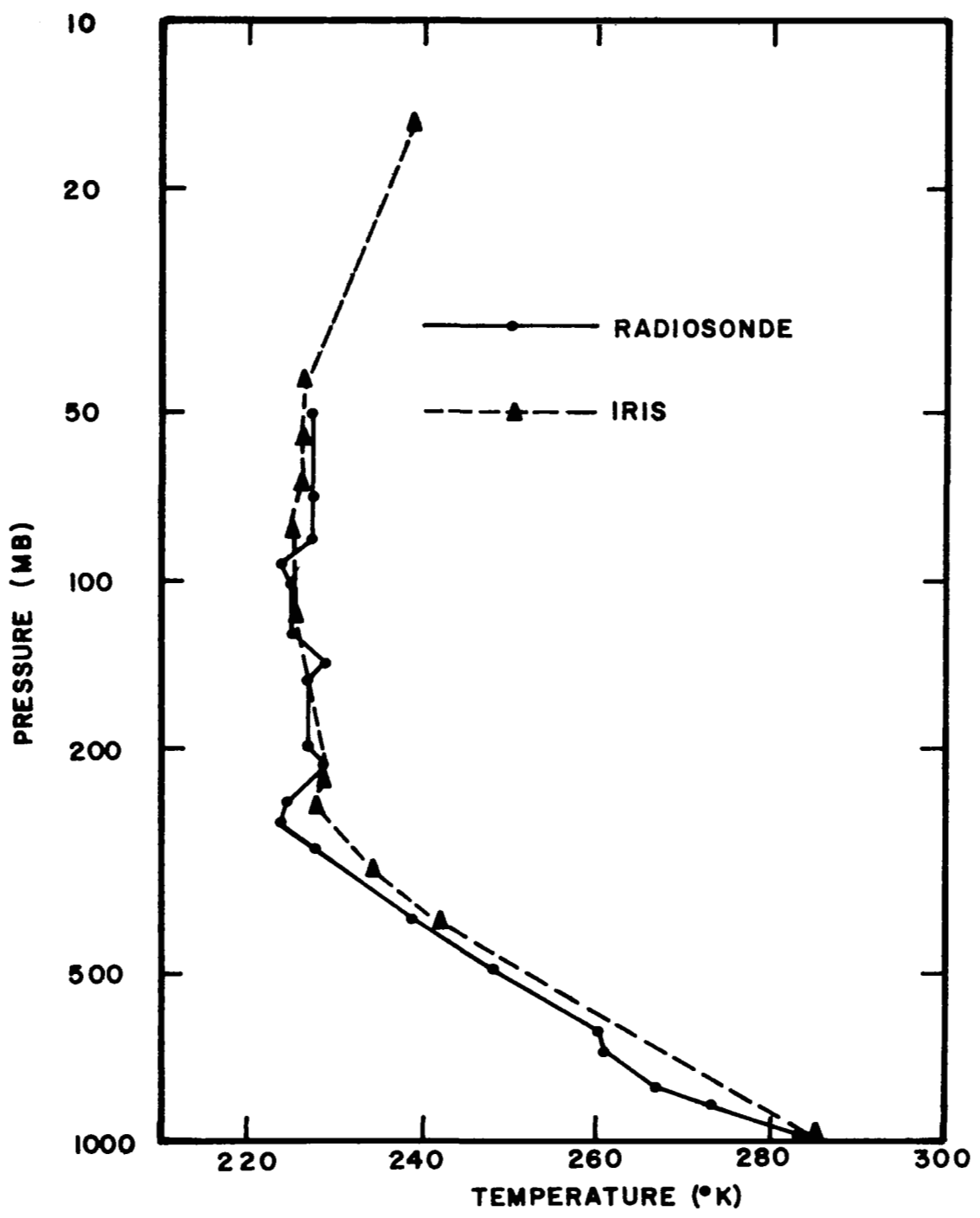


Figure 6. Comparison of a high latitude interpolated IRIS-computed temperature profile with a radiosonde sounding over Sodankyla, Finland, 1200 GMT, June 16, 1969.

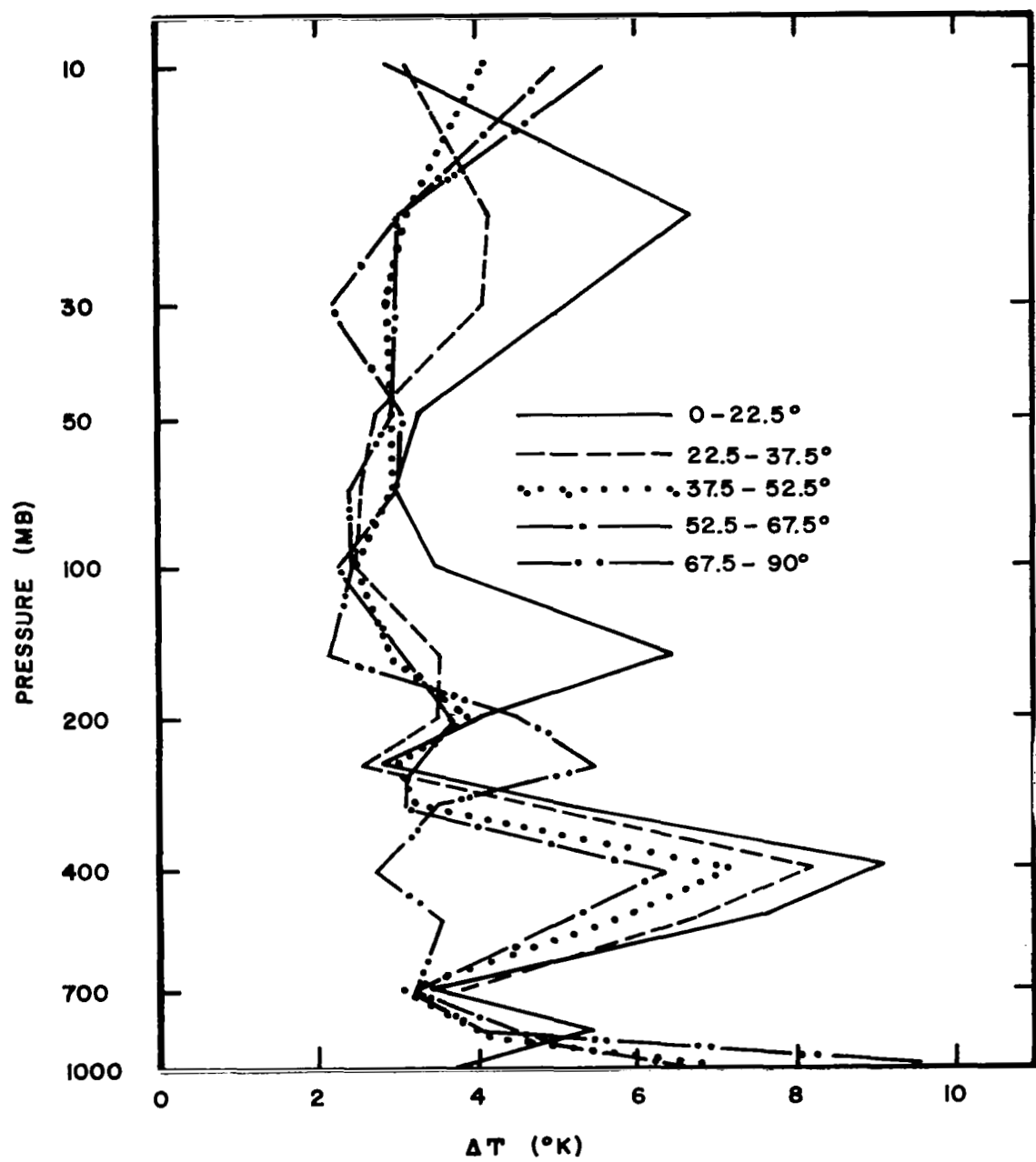


Figure 7. The RMS difference between interpolated IRIS-computed temperature profiles and radiosondes for five northern hemisphere latitude bands.

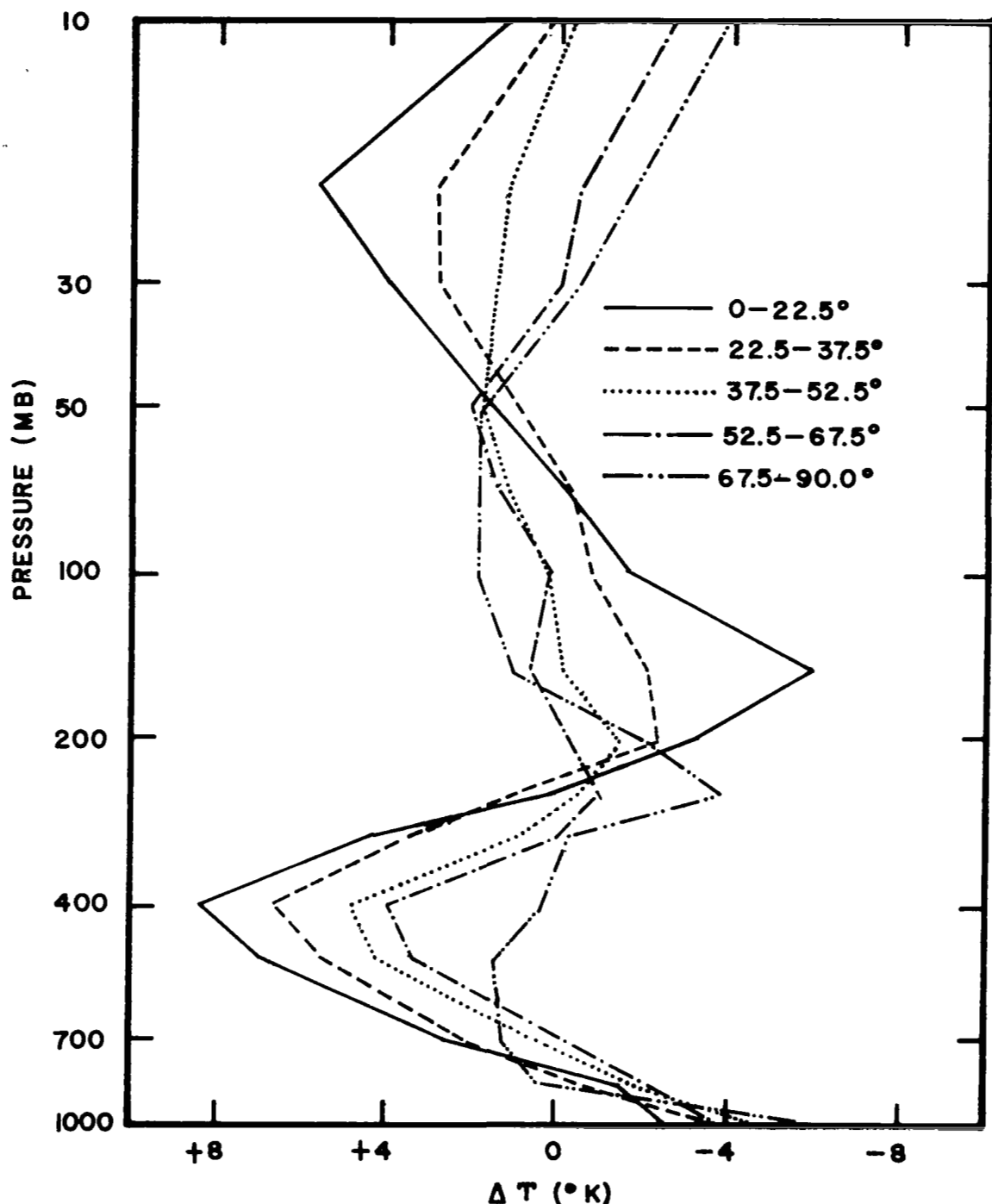


Figure 8. The average temperature difference (radiosonde temperature minus IRIS temperature) for five northern hemisphere latitude bands. The sample size for each latitude band is shown in Table 1.

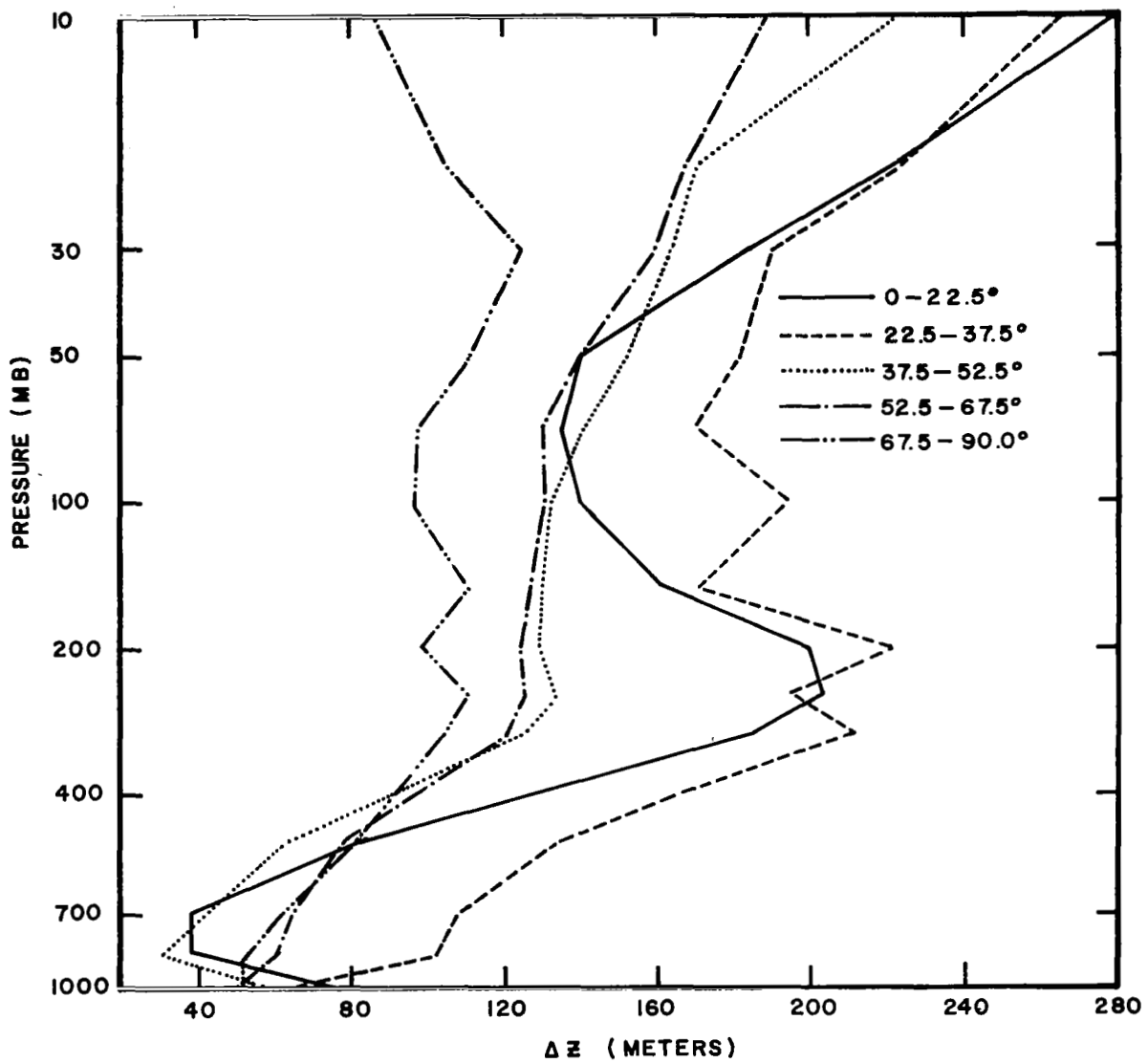


Figure 9(a). The RMS difference between interpolated IRIS-computed geopotential height profiles and radiosondes for five northern hemisphere latitude bands starting the integration of the hydrostatic equation at the earth's surface.

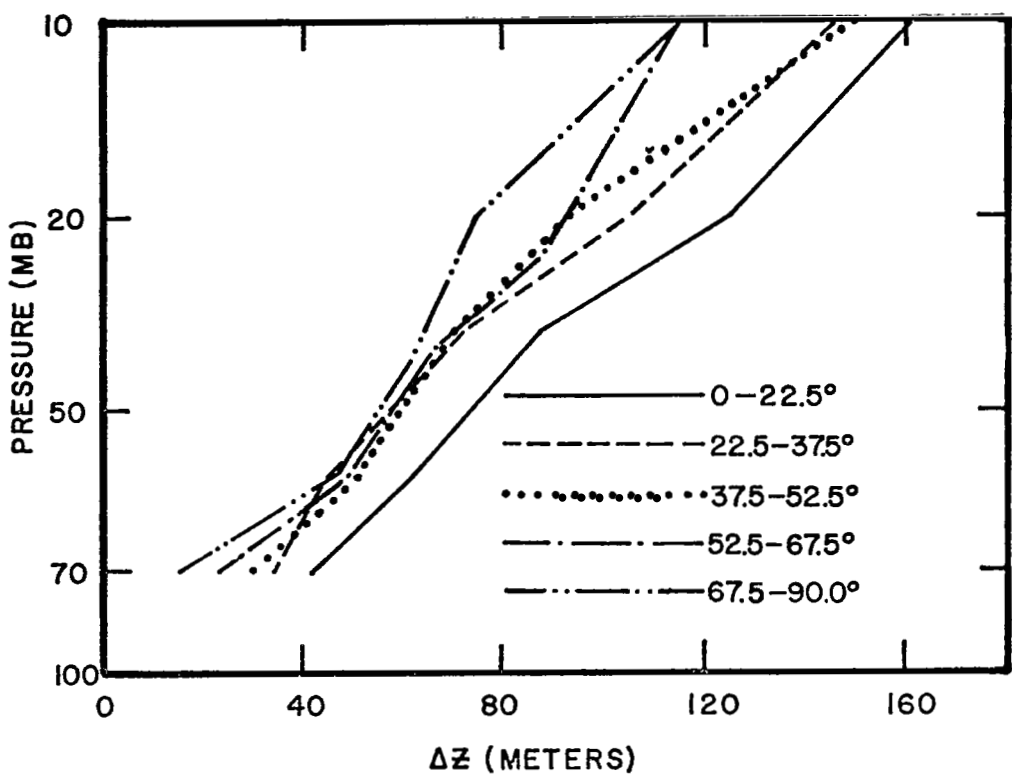


Figure 9(b). The RMS difference between interpolated IRIS-computed geopotential height profiles and radiosondes for five northern hemisphere latitude bands starting at the 100 mb level.

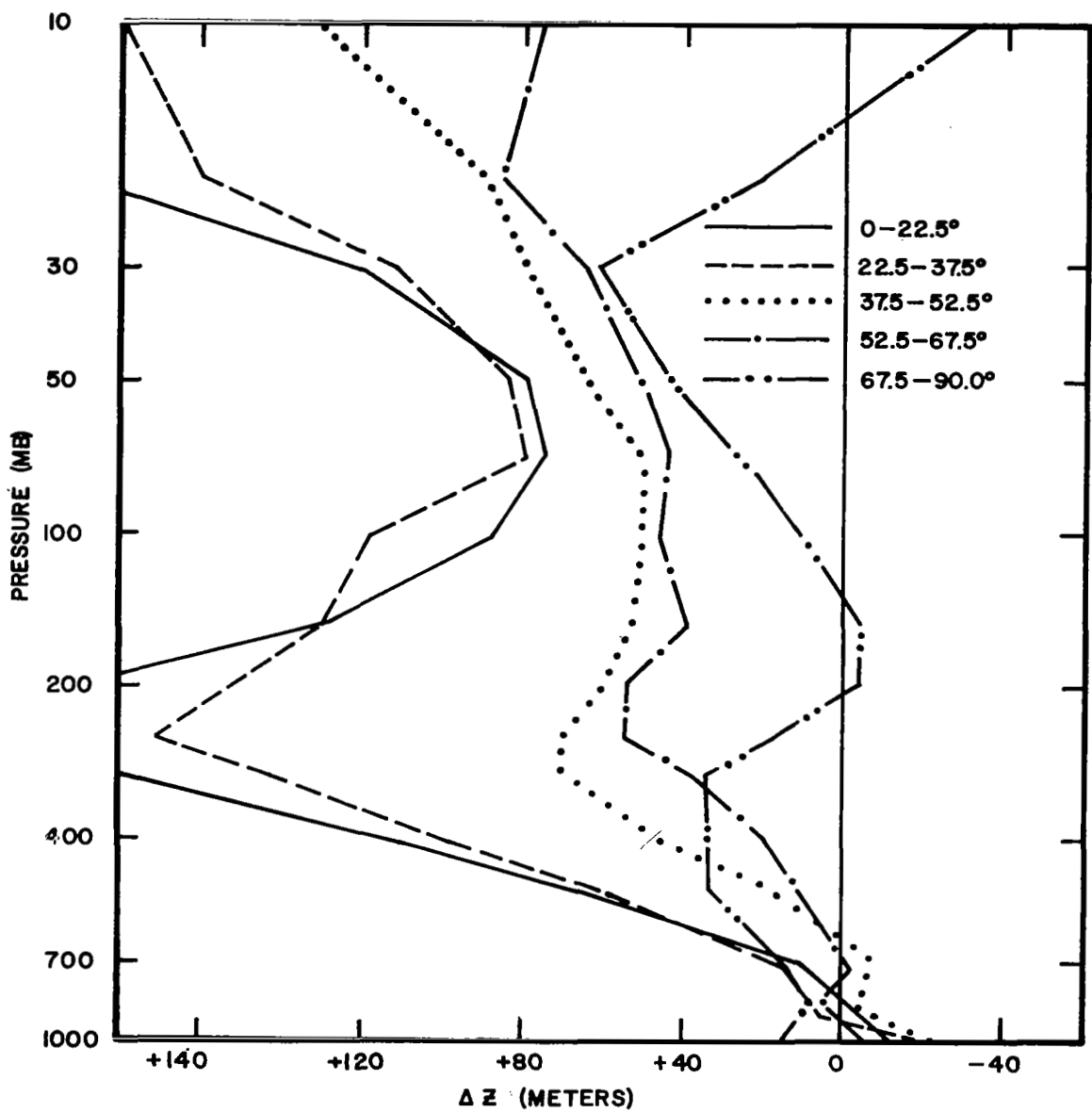


Figure 10(a). The average height difference (radiosonde height minus IRIS heights) for five northern hemisphere latitude bands starting the hydrostatic integration of the IRIS heights at the surface. The sample size for the latitude bands are shown in Table 1.

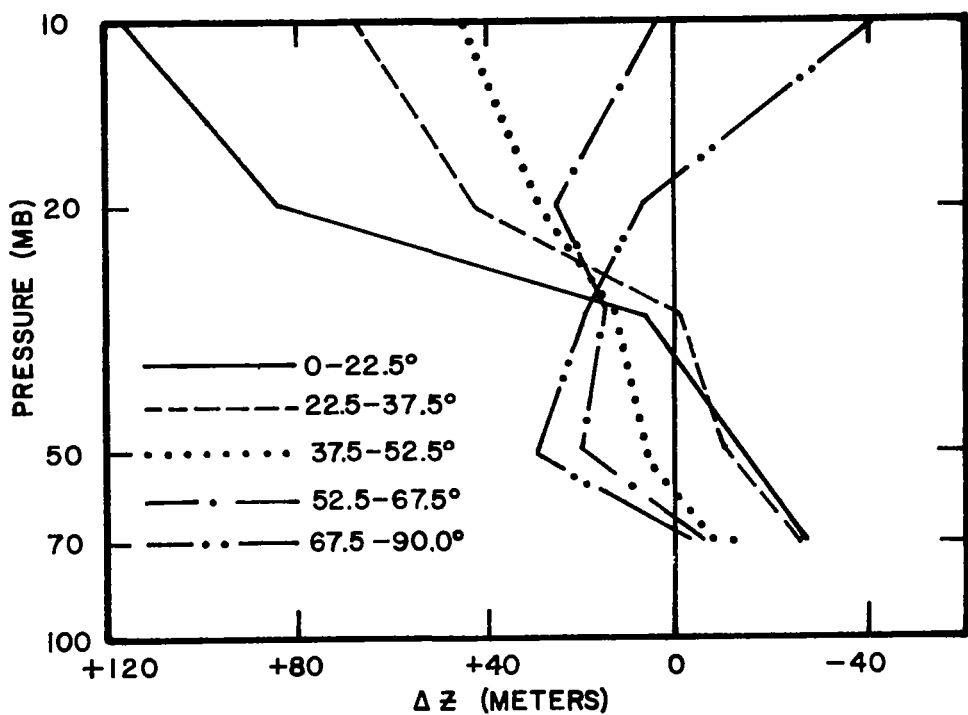


Figure 10(b). The average height difference (radiosonde height minus IRIS heights) for five northern hemisphere latitude bands starting at the 100 mb level. The sample size for the latitude bands are shown in Table 1.

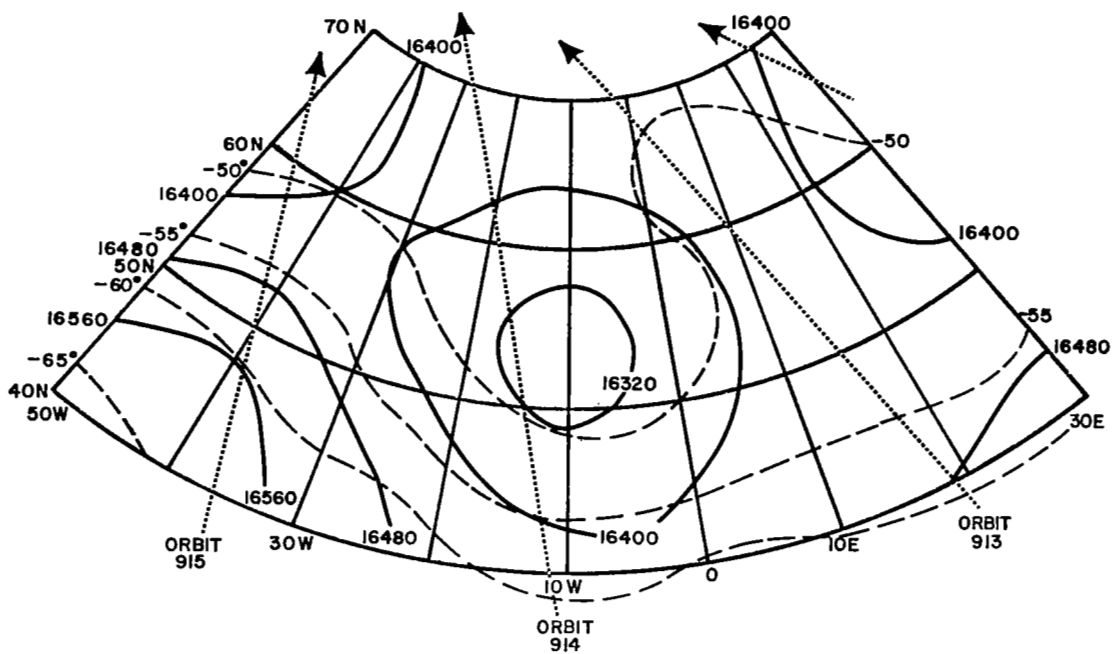


Figure 11. Portion of the NMC 100 mb map for 1200 GMT June 21, 1969. The solid lines are geopotential heights in meters and the dashed lines are temperatures in degrees C.

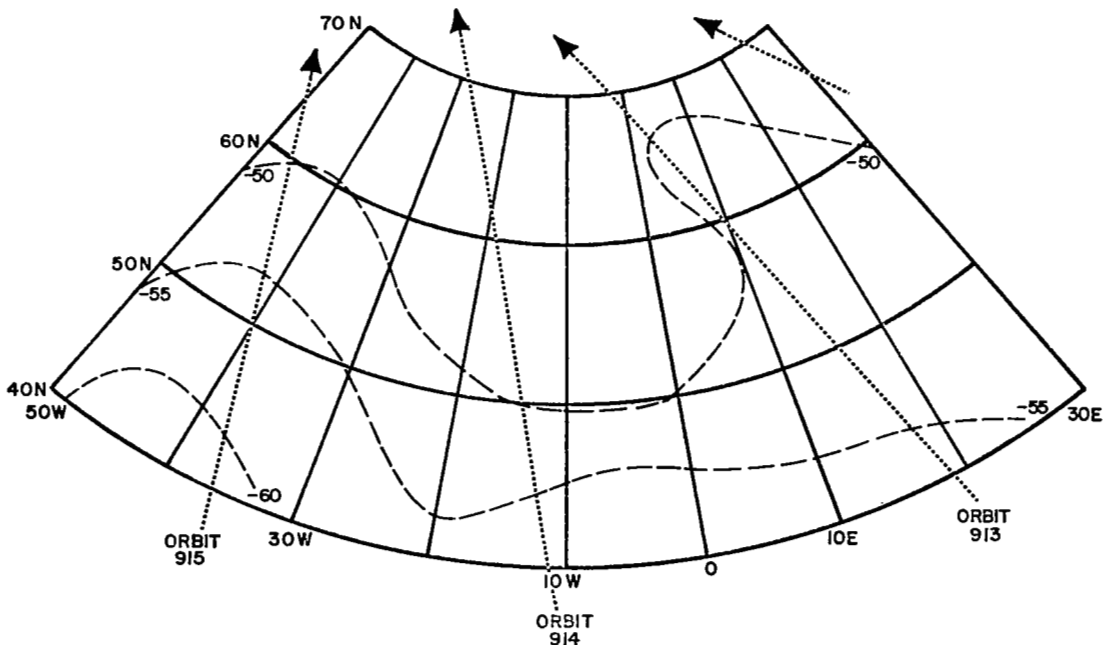


Figure 12. The 100 mb temperatures derived from interpolated IRIS. The data were acquired from the orbits shown: 913 from 0943 to 0952, 914 from 1130 to 1139, and 915 from 1317 to 1324 GMT

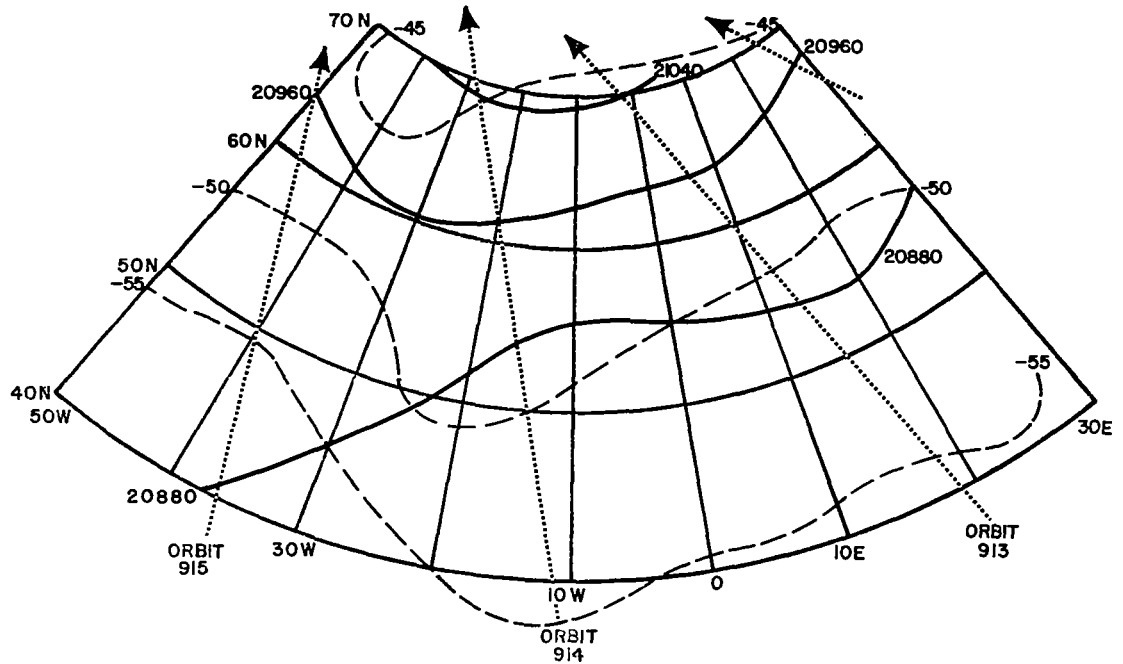


Figure 13. Portion of the NMC 50 mb map for 1200 GMT June 21, 1969. The solid lines are geopotential heights in meters and the dashed lines are temperatures in degrees C.

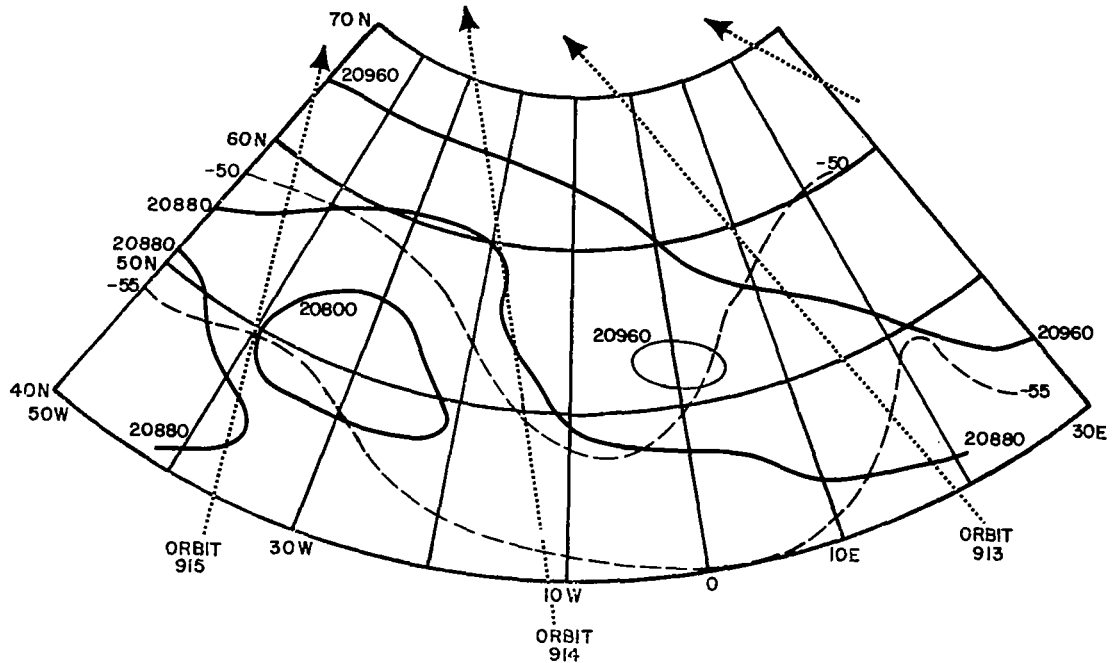


Figure 14. The 50 mb temperatures (dashed line) and heights (solid line) derived from interpolated IRIS.

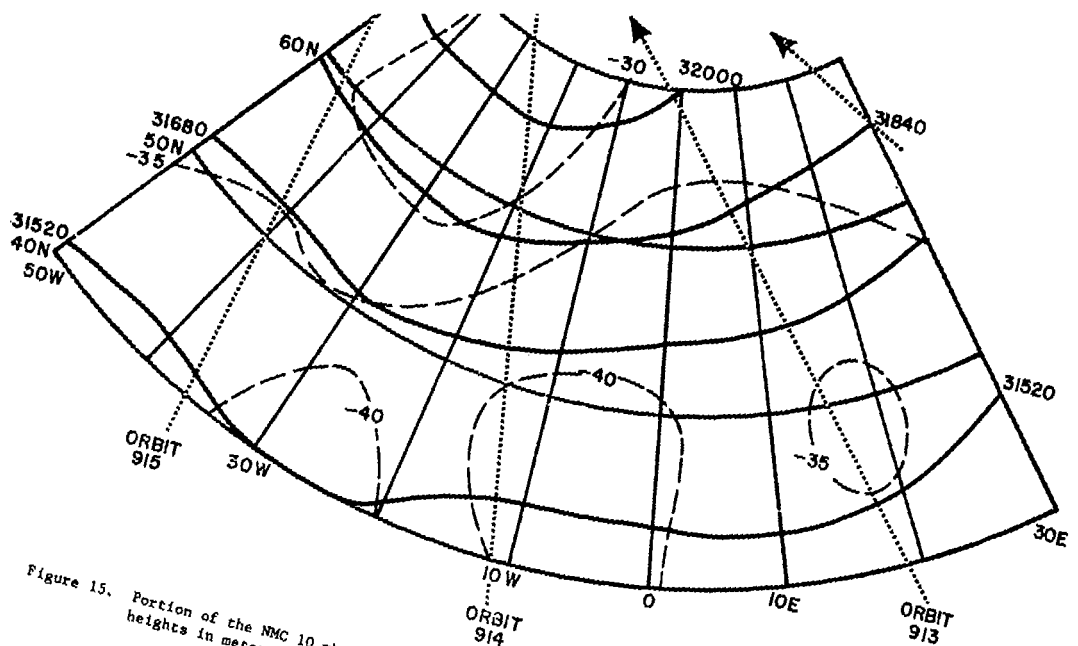


Figure 15. Portion of the NMC 10 mb map for 1200 GMT June 21, 1969. The solid lines are geopotential heights in meters and the dashed lines are temperatures in degrees C.

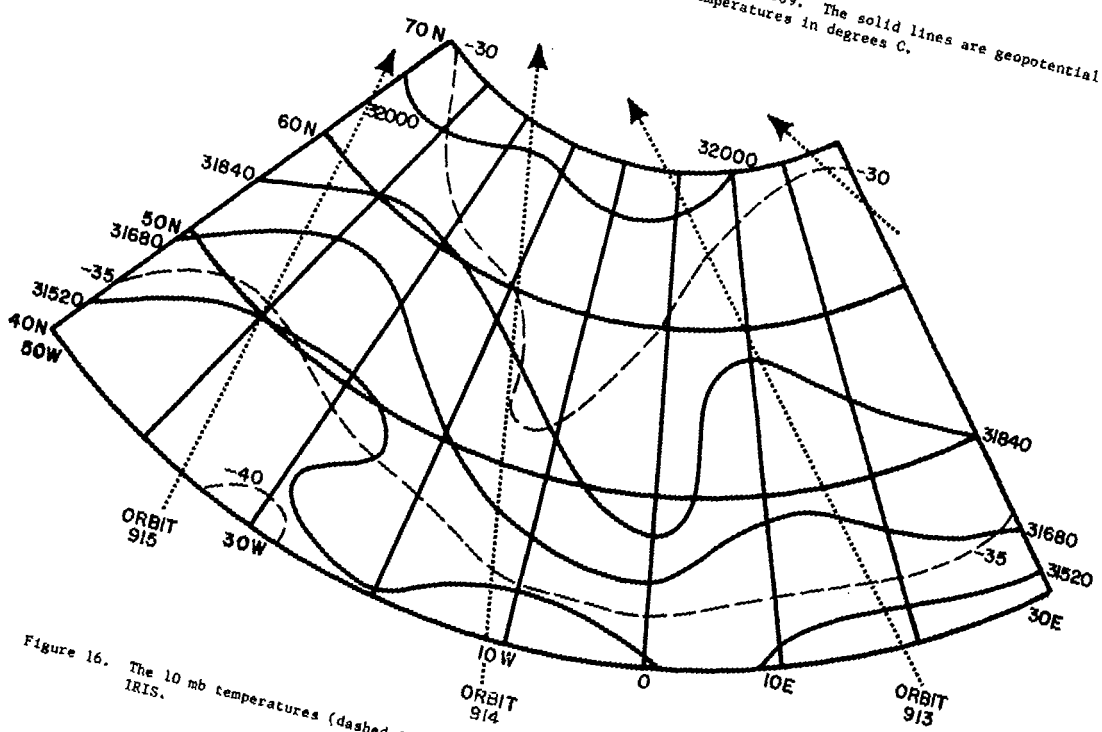


Figure 16. The 10 mb temperatures (dashed line) and heights (solid line) derived from interpolated IRIS.

Table 1. Correlation coefficients, R, for the interpolated IRIS computed temperature profiles and the radiosonde observed temperatures. The period is for June 15 to July 20, 1969. N is the sample size.

Pressure Level (mb)	0-22.5°		22.5-37.5°		37.5-52.5°		52.5-67.5°		67.5-90.0°		All Latitudes R
	N	R	N	R	N	R	N	R	N	R	
1000	61	.50	161	.38	291	.60	186	.65	32	.03	.71
850	72	.25	223	.54	522	.74	269	.73	33	.64	.77
700	74	.52	225	.51	525	.74	269	.72	33	.71	.82
500	74	.33	223	.23	521	.55	269	.47	33	.77	.68
400	74	.34	224	.36	523	.53	269	.38	33	.88	.62
300	74	.56	224	.61	523	.74	268	.57	33	.59	.80
250	51	.47	193	.68	453	.72	229	.62	19	.34	.78
200	73	.25	224	.54	525	.65	269	.78	32	.75	.67
150	73	.42	222	.72	520	.80	266	.62	33	.68	.89
100	74	.72	225	.86	525	.88	269	.67	33	.32	.96
70	72	.47	221	.66	516	.73	263	.44	33	.28	.92
50	67	.33	213	.28	497	.66	246	.42	33	.25	.87
30	64	.07	180	.14	388	.52	208	.53	27	.19	.75
20	55	.12	136	.25	323	.41	155	.50	23	.64	.64
10	36	.50	87	.22	170	.32	88	.30	7	.41	.59

Table 2. Correlation coefficients for the IRIS derived height profile and the radiosonde heights. The height profiles were computed by using the interpolated IRIS computed temperature profile starting with the radiosonde surface height and the 100-mb height. Period of sample was June 15 to July 20, 1969. The sample size is given in Table 1.

Pressure Level (mb)	Integration from Surface						Integration from 100 mb.					
	Latitude Bands						Latitude Bands					
	0 22.5 37.5 52.5 67.5 90.0	A11 Lat.	0 22.5 37.5 52.5 67.5 90.0	A11 Lat.								
1000	.454	.593	.635	.626	.633	.610						
850	.671	.524	.870	.711	.589	.708						
700	.585	.508	.833	.728	.589	.734						
500	.432	.449	.812	.749	.667	.783						
400	.385	.379	.782	.728	.723	.789						
300	.307	.313	.765	.706	.744	.794						
250	.378	.412	.775	.715	.716	.828						
200	.304	.302	.770	.642	.744	.802						
150	.232	.424	.720	.565	.684	.783						
100	.072	.083	.514	.475	.617	.478						
70	.182	.134	.308	.430	.595	.350	.842	.941	.965	.969	.980	.960
50	.286	.106	.253	.389	.595	.487	.581	.825	.896	.900	.904	.915
30	.325	.066	.266	.414	.429	.659	.463	.664	.809	.833	.735	.899
20	.365	.106	.343	.429	.566	.742	.141	.532	.750	.750	.706	.883
10	.481	.106	.387	.434	.858	.790	.392	.431	.628	.682	.718	.870